4. Design, synthesis, characterization and biological evaluation of eugenol/isoeugenol-derived carbohydrazones

4.1. Rationale, objectives and plan of work

4.1.1. Rationale

Eugenol is a naturally occurring phenolic compound possessing monoamine oxidase inhibitory potential. Apart from monoamine oxidase inhibition, eugenol also exhibits antioxidant, neuroprotective, antibacterial, anti-inflammatory and anticancer activity [108, 111, 114, 190]. The derivatives of eugenol show anticholinergic activity along with antioxidant activity [107, 109, 112, 113]. Hydrazones derived from eugenol are reported for anti-inflammatory and antibacterial activity [191]. Hydrazones (R-NH-N=C-R_1) are rich in hydrogen bond donors and acceptors which provide them an edge for more efficient molecular interaction. The hydrazone backbone has similarities with substrates of monoamine oxidase (e.g., dopamine). Several hydrazones and carbohydrazones are known to possess dual monoamine oxidases and acetylcholinesterase inhibitory potential [99, 192]. A study conducted by Nour *et al.* for the discovery of a promising cholinesterase inhibitor using eugenol derivates indicates the role of the allyl group in molecular interaction within the active site of AChE and BChE [193]. The current study is inspired by the dual inhibitory properties of the sesamol-derived extended carbohydrazone (compound **SMH06**, Chapter 2B), we envisaged incorporating or hybridizing the MAO-AChE inhibitory eugenol core to the carbohydrazone to derive a set of eugenol-carbohydrazone hybrids.

In other words, we replaced the benzodioxole core (sesamol) of **SMH06** with eugenol or isoeugenol core and explored the dual MAO-AChE inhibitory potential of the new eugenol-derived carbohydrazones. Focused variations were attempted at the imino terminal aryl ring

of the carbohydrazones. The design rationale is depicted in **Figure 4.1** and the 2D structures of eugenol/isoeugenol-derived carbohydrazone analogs are shown in **Figure 4.2**.

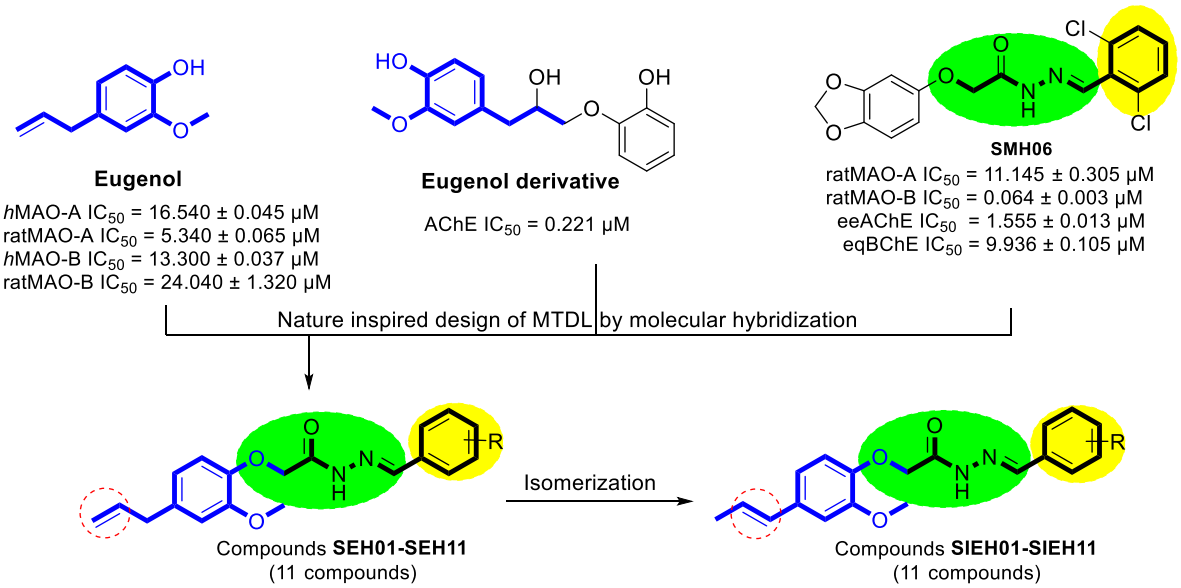

Figure 4.1. The design rationale for the design of eugenol-derived carbohydrazones

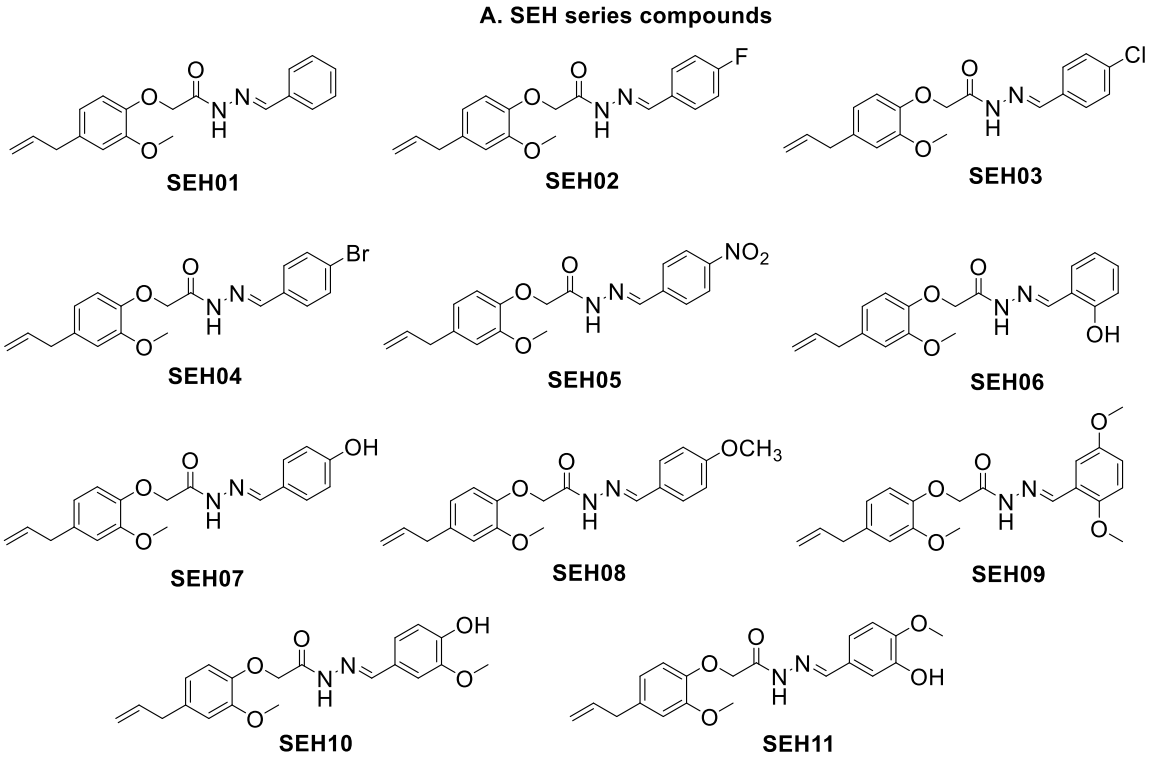

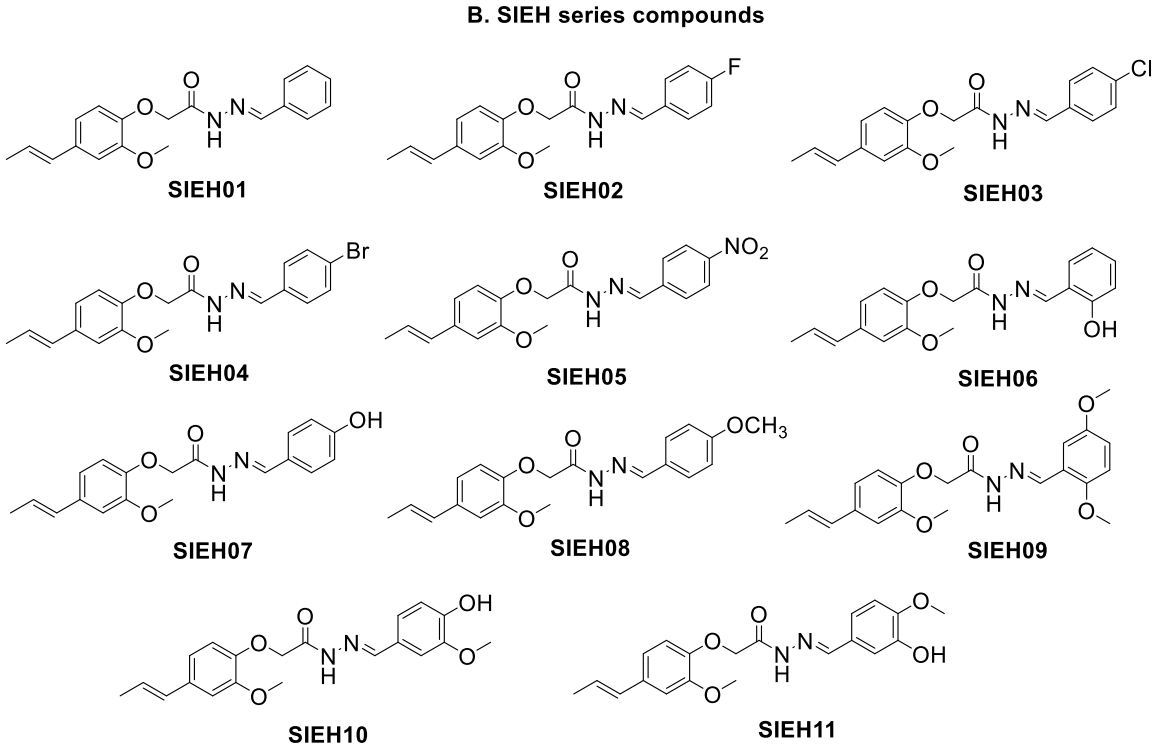

Figure 4.2. 2D chemical structure of designed compounds A) **SEH01-SEH11** & B) **SIEH01-SIEH11**

4.1.2. Objectives

- To design, synthesize and characterize a library of eugenol-derived carbohydrazones
- To perform the *in vitro* biological evaluation of synthesized compounds against MAOs (MAO-A/B) and ChEs (AChE and BChE) along with antioxidant and metal chelation assay of selected compounds
- To carry out the enzyme kinetics and reversibility studies of lead molecule(s) against MAO-B and AChE
- To perform the *in vitro* PAMPA-BBB assay of the lead molecules
- To evaluate the lead compound(s) for their *in vitro* cellular toxicity in fibroblast (L929) cells, neurotoxicity, and neuroprotective potential in neuroblastoma (SH-SY5Y) cell line

- To perform post-screening computational studies (MD simulation) and *in vivo* neuroprotective potential of lead molecule(s)

4.1.3. Plan of work

The plan of work for the design, synthesis and evaluation of the current series of compounds (**SEH01-SEH11** & **SIEH01-SIEH11**) is schematically presented in **Figure 4.3**. The lead optimization was performed using a scaffold hopping strategy where sesamol moiety was replaced with eugenol and isoeugenol moiety. A set of 22 new analogs was synthesized and evaluated by *in vitro*, *in cellulo*, *in vivo* and *ex vivo* studies for desired outcomes.

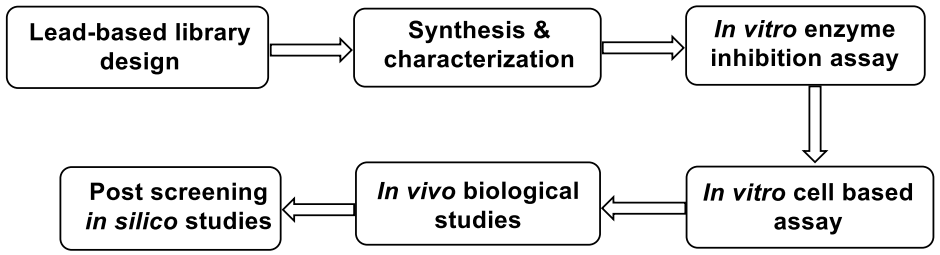

Figure 4.3. Overview of research workflow

4.2. Experimental Work

4.2.1. Chemistry

4.2.1.1. Synthesis

The chemicals and reagents utilized for synthesis purposes were procured from authentic sources. The synthetic reagents were obtained from Sigma-Aldrich Chemical Private Limited India, TCI India, Merck India, Fischer Scientific Ltd., Central Drug House (P) Ltd. India, Loba Chemie India, Sisco Research Laboratories (SRL) Pvt Ltd., and were used as such without any purification. The aluminium plates pre-coated with silica gel (Merck, Kieselgel 60F- 254, 0.20 mm) were used for monitoring the progress of the reaction.

Step 1: Synthesis of ethyl 2-(4-allyl-2-methoxyphenoxy)acetate (SEH IM 01) and ethyl (*E*)-2-(2-methoxy-4-(prop-1-en-1-yl)phenoxy)acetate (SIEH IM 01)

To a stirred solution of eugenol/isoeugenol (50 mmol) in acetone (50 mL), powdered and activated potassium carbonate (100 mmol) and ethyl bromoacetate (100 mmol) were added. The resulting reaction mixture was stirred at room temperature for 48 h. The progress of the reaction was monitored by TLC (20 % ethyl acetate: *n*-hexane). After completion of the reaction acetone was evaporated and the resultant residue was partitioned with ethyl acetate and water. The excess of ethyl bromoacetate in the solid product was removed by column chromatography (ethyl acetate: *n*-hexane 1:9). The synthetic scheme for intermediates **SEH IM 01** & **SIEH IM 01** is given in **Scheme 4.1**.

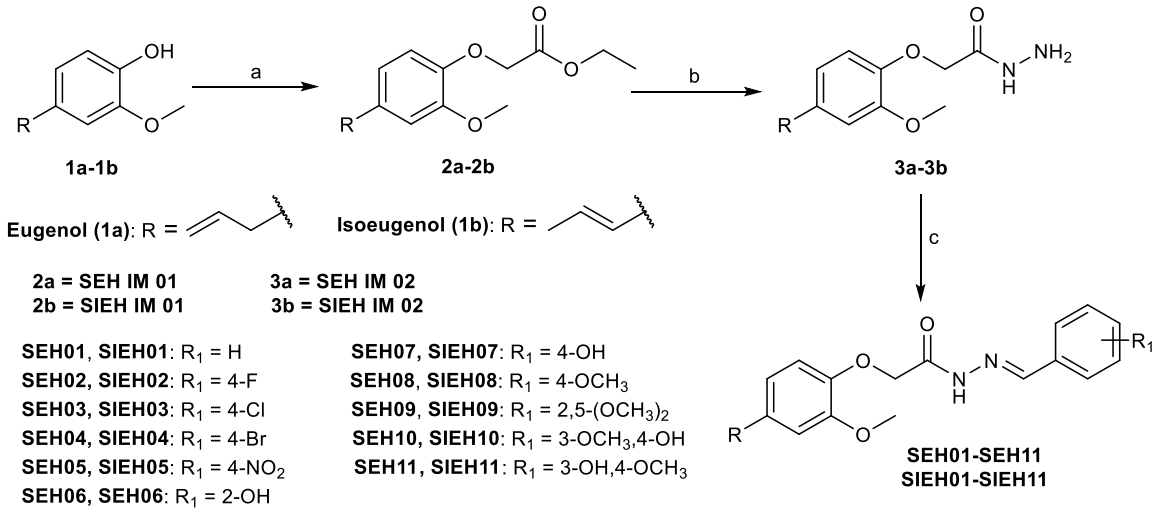

Scheme 4.1. Synthetic scheme for compounds **SEH01-SEH11** and **SIEH01-SIEH11**, Reagents and conditions: a), Ethyl bromoacetate, K_2CO_3, Acetone RT, 48 h, 95 % yield; b) Hydrazine hydrate, EtOH, reflux, 8 h, 92 % yield; c) substituted aldehydes, EtOH, RT, 2-5 h, 51-90 % yield.

Step 2: Synthesis of 2-(4-allyl-2-methoxyphenoxy)acetohydrazide (SEH IM 02) and (*E*)-2-(2-methoxy-4-(prop-1-en-1-yl)phenoxy)acetohydrazide (SIEH IM 02)

To a stirred solution of ethyl 2-(4-allyl-2-methoxyphenoxy)acetate (**SEH IM 01**, 50 mmol) or ethyl (*E*)-2-(2-methoxy-4-(prop-1-en-1-yl)phenoxy)acetate (**SIEH IM 01,** 50 mmol) in ethanol (50 mL) hydrazine hydrate (150 mmol) was added and the resulting reaction was refluxed for about 8 h. The progress of the reaction was monitored by TLC (60 % ethyl

acetate: *n*-hexane). After completion of the reaction, the mixture was cooled to 0 ºC and the resultant solid product was filtered under reduced pressure.

Step 3: General synthetic procedure of carbohydrazones (SEH01-SEH11 & SIEH01-SIEH11)

To a stirred solution of 2-(4-allyl-2-methoxyphenoxy)acetohydrazide (**SEH IM 02**, 1 mmol) or (*E*)-2-(2-methoxy-4-(prop-1-en-1-yl)phenoxy)acetohydrazide (**SIEH IM 02,** 1 mmol) in ethanol (10 mL) substituted aryl aldehyde (1.1 mmol) was added. The resulting reaction mixture was stirred at room temperature for about 2-5 h and the progress was monitored by TLC (40 % ethyl acetate: *n*-hexane). After completion of the reaction a portion of the mixture was evaporated and the remaining portion was cooled to 0 ºC and the obtained solid product was filtered under reduced pressure.

4.2.1.2. Physicochemical characterization

The final compounds were analyzed for solubility, retardation factor (R_f), and melting point, (**SEH01-SEH11** & **SIEH01-SIEH11**) by methodologies described earlier (**Section 2.3.2.**).

4.2.1.3. Spectral characterization

The chemical structure of the intermediates and final compounds (**SEH01-SEH11** & **SIEH01-SIEH11**) was confirmed and elucidated through spectroscopic techniques including FTIR, ^{1}H, ^{13}C NMR, MS and HRMS as described earlier (**Section 2.3.3**).

4.2.2. Biological studies

4.2.2.1. *In vitro* studies

4.2.2.1.1. *In vitro* MAO inhibition assay

The *in vitro* enzyme inhibition assay was performed to evaluate the inhibitory potential of compounds (**SEH01-SEH11** & **SIEH01-SIEH11**) against ratMAO-A and ratMAO-B. The

peroxidase-linked colorimetric method described by Holt *et al* was used for the MAO screening study. The assay is based on the colorimetric detection of 'quinoneimine dye' at 490 nm, formed by the reaction of vanillic acid and the oxidized product of 4-aminoantipyrine, the chromogenic substrate for this assay. The oxidation of 4-aminoantipyrine, in turn, is brought about by the action of MAO-A/B on its amine substrate i.e., serotonin and benzylamine, respectively, via the formation of the ROS (H_2O_2) through the cascade reaction. A complete protocol for MAO-A/B assay using a peroxidase-linked spectrometric method is mentioned in earlier section (**Section 2.4.1.1**)

4.2.2.1.2. *In vitro* ChEs inhibition assay

Test compounds (**SEH01-SEH11** & **SIEH01-SIEH11**) were screened against cholinesterases (*ee*AChE and *eq*BChE) using a well-known spectrometric method described by Ellman *et al.* The method is based on the hydrolysis of acetylthiocholine iodide (ATCI) and butyrylthiocholine iodide (BTCI) and the formation of nitro thiobenzoate (yellow) from 5,5-dithiobis(2-nitro benzoic acid) (DTNB) and thiocholine. The color intensity of the yellow complex of DTNB and thiocholine was measured at 415 nm. A detailed protocol for AChE and BChE enzyme inhibition is discussed in the previous section (**Section 2.4.1.3**).

4.2.2.1.3. Enzyme kinetics and reversibility

Enzyme kinetics of compound **SIEH10** was performed using different substrates (2.5, 5.0, 7.5, 10.0 and 15 mM) and inhibitor concentrations (1, 5 and 10 μM) by employing peroxidase-linked colorimetric method while time-dependent reversibility study was also performed to access the type of inhibitor. The AChE inhibitory mechanism of action of the lead compound **SIEH10**, reciprocal plots of 1/[V] versus 1/[S] was constructed using five different concentrations of the substrate acetylthiocholine iodide (ATCI) (0.5, 1.0, 1.5, 2.0, and 2.5 mM) using Ellman's method whereas the time-dependent reversibility study was

performed using variable incubation time up to 60 min. The detailed protocol followed for enzyme kinetics and reversibility study is given earlier (**Section 2.4.1.4**).

4.2.2.1.4. *In vitro* antioxidant assay

Antioxidant or free radical scavenging activity of selected test compounds along with donepezil, selegiline and tranylcypromine was performed by using 1,1-diphenyl-2-picrylhydrazyl (DPPH) assay. The method is based on the reductive capacity of a test molecule that can reduce 1,1-diphenyl-2-picrylhydrazyl (DPPH, deep purple color) to 1,1-diphenyl-2-picrylhydrazine (DPPH-H, pale yellow color) which shows absorbance at λ 517 nm. The detailed procedure for the antioxidant assay is discussed earlier (**Section 2.4.1.5**).

4.2.2.1.5. *In vitro* metal chelation assay

Iron chelation study of selected test compounds was carried out using the UV-based spectrophotometric method. An assay was performed in methanol while ferric chloride hexahydrate was used as a source of iron ions. The detailed procedure for metal chelation study is described earlier (**Section 2.4.1.6**)

4.2.2.1.6. *In vitro* blood-brain-barrier permeation assay

The *in vitro* blood-brain-barrier permeability assay of compound **SIEH10** was performed using PAMPA-BBB assay to evaluate the brain accessibility potential of the compound. The assay was carried out in a 96-well plate equipped with a microfilter device at its bottom and coated with a hydrophobic material (porcine brain lipid) that mimics BBB. A detailed step-by-step protocol for PAMPA-BBB assay is discussed earlier (**Section 2.4.1.7**).

4.2.2.1.7. Cell-based neurotoxicity assay

Compound **SIEH10** was evaluated for its cytotoxicity in fibroblast (L929) cells and for possible neurotoxicity in the neuroblastoma cell line (SH-SY5Y). The cells were treated with the different concentrations (0.1, 1, 10, 50 and 100 μM) of the test compound for 24

h. Further, an MTT assay was performed to estimate the percent cell viability. A detailed method for cell culture and MTT assay is described earlier (**Section 2.4.1.8**)

4.2.2.1.8. Neuroprotection assay using neuroblastoma cell line

The neuroprotective potential of compound **SIEH10** was evaluated against dexamethasone-induced oxidative stress and apoptosis. The cells were treated for 3 days (72 h) with different concentrations (0.25, 100 and 200 nM) of compound **SIEH10** prepared in media containing 2 μM of dexamethasone (HiMedia Laboratories Private Limited, India, Cat. TCL211) solution. Furthermore, an MTT assay was performed to assess the cell survival and neuroprotective potential of the compound. A more detailed method is described earlier (**Section 2.4.1.9**).

4.2.2.2. *In vivo* studies

4.2.2.2.1. Scopolamine-induced amnesia model (Y-maze test)

The *in vivo* neuroprotective efficacy of the compound **SIEH10** was evaluated using the scopolamine-induced amnesia model and Y-maze test. A 7-day prophylactic treatment of 5 mg/kg (i.p.) of test compound **SIEH10** and 5 mg/kg (i.p.) of donepezil was given to the mice and on the 7^{th} day animals were treated with 3 mg/kg (i.p.) of scopolamine 30 min post-treatment with test compound or vehicle. After 15 min of scopolamine administration, the animals were subjected to a Y-maze test. The spontaneous alteration behavior of each animal was recorded and the obtained results were analyzed. A detailed experimental protocol for scopolamine-induced amnesia and the Y-maze test is described earlier (**Section 2.4.2.1** and **2.4.2.2**).

4.3. Computational studies

4.3.1. Molecular docking

Molecular docking studies of all the test compounds **SEH01-SEH11** & **SIEH01-SIEH11** and co-crystallized inhibitors were carried out using AutoDock Tools 4.2 (ADT) (The Scripps Research Institute, California, USA). A detailed description of the *in silico* molecular docking studies and docked pose analysis is presented in **Section 2.5.1**.

4.3.2. Molecular dynamics simulation

A molecular dynamic simulation of the selected compound was performed using Desmond (Schrodinger Release 2021.1). Preparation of input files from the protein-ligand complex and analysis of simulated results and trajectory analysis were completed in the Maestro graphical user interface (Maestro, Schrodinger, LLC, New York, NY, 2021). The detailed protocol for molecular dynamic simulation using Desmond is discussed earlier (**Section 2.5.2**) [15, 122].

4.3.3. Ligand binding efficiency

Ligand binding efficiency for all the synthesized compounds **SEH01-SEH11** & **SIEH01-SIEH11** along with reference inhibitors (clorgyline, selegiline and donepezil) was calculated from a web-based server (MedChem calculators) by feeding the experimental IC_{50} value and number of heavy atoms (http://www.vulpinescience.co.uk/uploads/MedChem%20Calculators_Ver3.2/MedChem%20Calculators.htm) accessed on 07 October 2024 [29].

4.3.4. Predicted ADMET properties

Compounds **SEH01-SEH11** & **SIEH01-SIEH11** were screened for *in silico* ADMET (absorption, distribution, metabolism, excretion and toxicity) properties prediction. The 'PreADMET' server (Web-based) was used for the calculation of ADMET parameters. The

server employs various algorithms for ADME and toxicity prediction (https://preadmet.bmdrc.kr/). The .mol coordinates of each compound were generated from sketched 2D chemical structures and fed into the PreADMET server for properties calculation [176, 194].

4.4. Results and Discussion

4.4.1. Chemistry

4.4.1.1. Physicochemical characterization of final compounds

All the final compounds of **SEH & SIEH series** derived from eugenol and isoeugenol (**SEH01-SEH11** & **SIEH01-SIEH11**) were synthesized by reaction of eugenol/isoeugenol with ethyl bromoacetate which yielded ester derivative and the reaction of ester with hydrazine hydrate led to the formation of respective carbohydrazide of eugenol and isoeugenol. These hydrazides upon reaction with different aldehyde derivatives resulted in the final compounds. The determined physicochemical properties are listed in **Table 4.1**.

Most of the compounds of **SEH** and **SIEH series** were obtained while solid and were freely soluble in dichloromethane (DCM), ethyl acetate, and chloroform same as compound **SMH06** while calculated logP values of most of the molecules were greater than compound **SMH06** which may improve the lipophilicity of the compounds.

Table 4.1. Physicochemical characterization results of compounds **SEH01-SEH11** & **SIEH01-SIEH11**

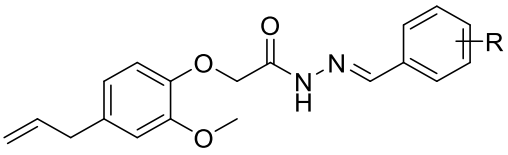

SEH01-SEH11

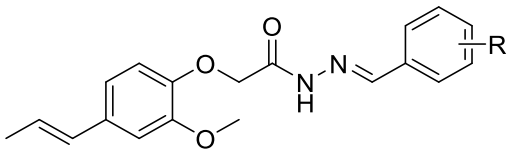

SIEH01-SIEH11

Compd. code	R	MW	ClogP[a]	Yield (%)	MP (°C)	R_f[b]	Solubility	Appearance
SEH01	H	324.38	3.49	40.00	75-77	0.85	A	White solid

SEH02	4-F	342.37	3.63	68.00	103-105	0.85	A	White solid
SEH03	4-Cl	358.82	4.20	55.00	97-99	0.88	A	White solid
SEH04	4-Br	403.27	4.35	57.00	108-110	0.88	A	White solid
SEH05	4-NO_2	369.37	3.23	70.00	125-127	0.80	A	Off-white solid
SEH06	2-OH	340.37	4.09	51.00	90-92	0.95	A	White solid
SEH07	4-OH	340.37	3.46	69.00	74-76	0.54	A	Brown solid
SEH08	4-OCH_3	354.40	3.71	51.00	68-70	0.77	A	White solid
SEH09	2,5-di-OCH_3	384.43	3.35	69.00	99-101	0.67	A	White solid
SEH10	3-OCH_3, 4-OH	370.40	3.28	65.00	-[c]	0.51	A	Off-white solid
SEH11	3-OH, 4-OCH_3	370.40	3.28	67.00	-[c]	0.51	A	Pale yellow solid
SIEH01	H	324.38	3.68	85.00	109-111	0.87	A	White solid
SIEH02	4-F	342.37	3.82	90.00	130-132	0.84	A	White solid
SIEH03	4-Cl	358.82	4.39	70.00	130-132	0.87	A	White solid
SIEH04	4-Br	403.27	4.54	83.00	135-137	0.89	A	White solid
SIEH05	4-NO_2	369.37	3.42	76.00	147-149	0.79	A	Off-white solid
SIEH06	2-OH	340.37	4.28	79.00	122-124	0.97	A	Off-white solid
SIEH07	4-OH	340.37	3.65	81.00	151-153	0.50	A	Off-white solid
SIEH08	4-OCH_3	354.40	3.90	66.00	126-128	0.75	A	White solid
SIEH09	2,5-di-OCH_3	384.43	3.35	78.00	111-113	0.82	A	White solid
SIEH10	3-OCH_3, 4-OH	370.40	3.47	70.00	90-92	0.50	A	White solid
SIEH11	3-OH, 4-OCH_3	370.40	3.47	50.00	138-140	0.50	A	Pale yellow solid

[a] Calculated from ChemDraw 17.1.0; [b] TLC Mobile Phase: Ethyl acetate**:** *n*-hexane (6:4); [c] Sticky solid; **A** = soluble in Chloroform, DCM, ethyl acetate and methanol.

4.4.1.2. Spectral characterization of final compounds

The synthesized molecules of the **SEH series** (**SEH01-SEH11**) and **SIEH series** (**SIEH01-SIEH11**) were characterized by different analytical techniques (FTIR, ^{1}H, ^{13}C NMR, MS, and HRMS) to ensure and prove the concept and process involved in the synthesis. The conversion of eugenol/isoeugenol to ester derivative was confirmed by the disappearance of the peak due to the hydroxyl group in the region of ν 4000 cm^{-1} to ν 3300 cm^{-1} in FTIR spectra, while in NMR it was proved by the presence of a singlet peak of methylene protons in the region between δ 4-5 ppm in ^{1}H NMR whereas near δ 70 ppm in ^{13}C NMR. The formation of hydrazide from the ester of eugenol/isoeugenol was confirmed due to the presence of a stretching peak of amine NH in the region of ν 3500 cm^{-1} to ν 3100 cm^{-1}, while in ^{1}H NMR it was confirmed by the presence of singlet peak due to amide NH in the range of δ 9-10 ppm. The presence of a peak at 237 m/z ratio (M+1) in mass spectra also

the conversion of ester to hydrazide. The formation of hydrazone was confirmed by peak due to imine functional group in FTIR spectra in the range of *v* 1690 cm^{-1} to *v* 1640 cm^{-1}, while in ^{1}H NMR it was confirmed by the presence of singlet peak near *δ* 8 ppm and in ^{13}C NMR near *δ* 145 ppm. The presence of molecular ion peak (M-1) in the mass spectra and HRMS of each molecule ensured the formation of the hydrazones. The allyl CH protein of eugenol analogs appears as multiplet near *δ* 6 ppm while in isoeugenol analogs two multiplet appear between *δ* 6-6.5 ppm due to two alkene CH protons.

Ethyl 2-(4-allyl-2-methoxyphenoxy)acetate (SEH IM 01): ^{1}H NMR (500 MHz, $CDCl_3$) *δ* ppm 6.78 (d, *J* = 8.1 Hz, 1H), 6.75 (d, *J* = 2.1 Hz, 1H), 6.70 (d, *J* = 10.2 Hz, 1H), 5.96 (ddt, *J* = 16.9, 10.1, 6.7 Hz, 1H), 5.15 – 5.03 (m, 2H), 4.67 (s, 2H), 4.26 (q, *J* = 7.2 Hz, 2H), 3.88 (s, 3H), 3.34 (d, *J* = 6.7 Hz, 2H), 1.29 (t, *J* = 7.1 Hz, 3H); ^{13}C NMR (126 MHz, $CDCl_3$) *δ* ppm 169.19, 149.57, 145.63, 137.47, 134.47, 120.39, 115.79, 114.55, 112.54, 66.77, 61.23, 55.85, 39.84, 14.18.

Ethyl (*E*)-2-(2-methoxy-4-(prop-1-en-1-yl)phenoxy)acetate (SIEH IM 01): ^{1}H NMR (500 MHz, $CDCl_3$) *δ* ppm 6.92 (d, *J* = 2.0 Hz, 1H), 6.84 (dd, *J* = 8.4, 2.0 Hz, 1H), 6.77 (d, *J* = 8.2 Hz, 1H), 6.35 (d, *J* = 15.7 Hz, 1H), 6.14 (dd, *J* = 15.6, 6.6 Hz, 1H), 4.68 (s, 2H), 4.27 (q, *J* = 7.2 Hz, 2H), 3.91 (s, 3H), 1.88 (d, *J* = 1.7 Hz, 3H), 1.30 (t, *J* = 7.1 Hz, 3H); ^{13}C NMR (126 MHz, $CDCl_3$) *δ* ppm 169.09, 149.62, 146.35, 132.81, 130.46, 124.56, 118.45, 114.37, 109.27, 66.69, 61.29, 55.85, 18.39, 14.18.

2-(4-Allyl-2-methoxyphenoxy)acetohydrazide (SEH IM 02): ^{1}H NMR (500 MHz, $CDCl_3$) *δ* ppm 8.31 (s, 1H), 6.81 (t, *J* = 8.2 Hz, 1H), 6.77 – 6.70 (m, 2H), 5.95 (ddt, *J* = 16.9, 10.2, 6.7 Hz, 1H), 5.17 – 5.00 (m, 2H), 4.59 (s, 2H), 3.88 (s, 4H), 3.34 (d, *J* = 6.7 Hz, 1H), 2.61 – 2.48 (m, 1H), 1.69 – 1.56 (m, 1H), 0.95 (t, *J* = 7.3 Hz, 1H); ^{13}C NMR (126

MHz, $CDCl_3$) δ ppm 169.10, 149.58, 145.40, 138.09, 137.22, 135.34, 120.77, 116.01, 112.50, 69.44, 55.87, 39.84.

(*E*)-2-(2-methoxy-4-(prop-1-en-1-yl)phenoxy)acetohydrazide (SIEH IM 02): ^{1}H NMR (500 MHz, $CDCl_3$) δ ppm 8.20 (s, 1H), 6.93 (d, J = 2.1 Hz, 1H), 6.88 (dd, J = 8.2, 2.1 Hz, 1H), 6.83 (d, J = 8.4 Hz, 1H), 6.36 (d, J = 17.4 Hz, 1H), 6.22 – 6.11 (m, 1H), 4.62 (s, 2H), 3.92 (s, 5H), 1.89 (s, 3H); ^{13}C NMR (126 MHz, $CDCl_3$) δ ppm 169.03, 149.65, 145.99, 133.59, 130.25, 125.23, 118.75, 115.38, 109.15, 69.30, 55.79, 18.42.

(*E*)-2-(4-allyl-2-methoxyphenoxy)-*N′*-benzylidene acetohydrazide (SEH01) [191, 195, 196]: White solid; Yield: 40 %; MP: 75-77 ºC; R_f: 0.85 in 60 % ethyl acetate-*n*-hexane; FTIR (KBr, *v,* cm^{-1}): 3192 (amide NH str), 3072 (aromatic CH str), 2973 (aliphatic CH_2 str), 1685 (C=O), 1636 (C=N str), 1515 (aromatic C=C str); ^{1}H NMR (500 MHz, $CDCl_3$) δ ppm 10.16 (s, 1H, amide-NH), 8.17 (s, 1H, imine-CH), 7.84 – 7.76 (m, 2H), 7.43 (dd, J = 5.2, 2.0 Hz, 3H), 6.93 (d, J = 7.9 Hz, 1H), 6.79 (d, J = 8.9 Hz, 2H), 6.06 – 5.90 (m, 1H), 5.17 – 5.04 (m, 2H), 4.72 (s, 2H, -CH_2), 3.95 (s, 3H, -OCH_3), 3.38 (d, J = 6.7 Hz, 2H); ^{13}C NMR (126 MHz, $CDCl_3$) δ ppm 165.13 (-C=O), 149.63, 149.07, 145.55 (-C=N), 137.13, 135.91, 133.34, 130.74, 128.71, 127.88, 121.28, 116.65, 116.13, 112.68, 70.33 (-CH_2), 55.88 (-OCH_3), 39.87; MS (ESI$^-$): *m/z* = 323.05 $(M-1)^-$; HRMS calcd for $C_{19}H_{20}N_2O_3$ $(M+H)^+$ 325.1552, found 325.1548.

(*E*)-2-(4-allyl-2-methoxyphenoxy)-*N′*-(4-fluorobenzylidene)acetohydrazide (SEH02) [191]: White solid; Yield: 68 %; MP: 103-105 ºC; R_f: 0.85 in 60 % ethyl acetate-*n*-hexane; FTIR (KBr, *v,* cm^{-1}): 3190 (amide NH str), 3074 (aromatic CH str), 2970 (aliphatic CH_2 str), 1685 (C=O), 1638 (C=N str), 1516 (aromatic C=C str), 1146 (aryl C-F str); ^{1}H NMR (500 MHz, $CDCl_3$) δ ppm 10.14 (s, 1H, amide-NH), 8.17 (s, 1H, imine-CH), 7.79 (dd, J = 8.9, 5.4 Hz, 2H), 7.11 (t, J = 8.6 Hz, 2H), 6.93 (d, J = 7.9 Hz, 1H), 6.81 – 6.70 (m, 2H),

6.10 – 5.76 (m, 1H), 5.16 – 5.05 (m, 2H), 4.71 (s, 2H, -CH_2), 3.94 (s, 3H, -OCH_3), 3.37 (d, *J* = 6.7 Hz, 2H); ^{13}C NMR (126 MHz, $CDCl_3$) δ ppm 165.16 (-C=O), 163.24, 149.62, 147.82, 145.52 (-C=N), 137.11, 135.94, 129.80, 129.73, 121.28, 116.63, 116.14, 116.01, 115.84, 112.70, 70.29 (-CH_2), 55.89 (-OCH_3), 39.86; MS (ESI^-): *m/z* = 341.05 $(M-1)^-$; HRMS calcd for $C_{19}H_{19}FN_2O_3$ $(M+H)^+$ 343.1458, found 343.1458.

(*E*)-2-(4-allyl-2-methoxyphenoxy)-*N′*-(4-chlorobenzylidene)acetohydrazide (SEH03) [191, 196]: White solid; Yield: 55 %; MP: 97-99 ºC; R_f: 0.88 in 60 % ethyl acetate-*n*-hexane; FTIR (KBr, *v,* cm^{-1}): 3187 (amide NH str), 3073 (aromatic CH str), 2967 (aliphatic CH_2 str), 1684 (C=O), 1516 (aromatic C=C str), 1088 (Aryl C-Cl str); ^{1}H NMR (500 MHz, $CDCl_3$) δ ppm 10.17 (s, 1H, amide-NH), 8.16 (s, 1H, imine-CH), 7.73 (d, *J* = 8.5 Hz, 2H), 7.40 (d, *J* = 8.5 Hz, 2H), 6.93 (d, *J* = 7.9 Hz, 1H), 6.79 (d, *J* = 8.4 Hz, 2H), 6.08 – 5.87 (m, 1H), 5.15 – 5.06 (m, 2H), 4.71 (s, 2H), 3.95 (s, 3H, -OCH_3), 3.38 (d, *J* = 6.7 Hz, 2H); ^{13}C NMR (126 MHz, $CDCl_3$) δ ppm 165.21 (-C=O), 149.63, 147.68, 145.51 (-C=N), 137.11, 136.66, 135.98, 131.92, 129.04, 128.99, 121.30, 116.67, 116.16, 112.71, 70.32 (-CH_2), 55.88 (-OCH_3), 39.87; MS (ESI^-): *m/z* = 357.00 $(M-1)^-$; HRMS calcd for $C_{19}H_{19}ClN_2O_3$ $(M+H)^+$ 359.1162, found 359.1150.

(*E*)-2-(4-allyl-2-methoxyphenoxy)-*N′*-(4-bromobenzylidene)acetohydrazide (SEH04) [191]: White solid; Yield: 57 %; MP: 108-110 ºC; R_f: 0.88 in 60 % ethyl acetate-*n*-hexane; FTIR (KBr, *v,* cm^{-1}): 3082 (aromatic CH str), 2962 (aliphatic CH_2 str), 1683 (C=O), 1516 (aromatic C=C str), 1036 (aryl C-Br str); ^{1}H NMR (500 MHz, $CDCl_3$) δ ppm 10.18 (s, 1H, amide-NH), 8.15 (s, 1H, imine-CH), 7.67 (d, *J* = 8.5 Hz, 2H), 7.56 (d, *J* = 8.5 Hz, 2H), 6.93 (d, *J* = 8.2 Hz, 1H), 6.79 (d, *J* = 7.9 Hz, 2H), 6.05 – 5.86 (m, 1H), 5.20 – 5.07 (m, 2H), 4.71 (s, 2H, -CH_2), 3.95 (s, 3H, -OCH_3), 3.38 (d, *J* = 6.7 Hz, 2H); ^{13}C NMR (126 MHz, $CDCl_3$) δ ppm 165.21 (-C=O), 149.61, 147.75, 145.49 (-C=N), 137.10, 135.98, 132.35, 131.99, 129.19, 125.07, 121.31, 116.64, 116.16, 112.72, 70.30 (-CH_2), 55.91 (-OCH_3), 39.86; MS

(ESI⁻): *m/z* = 401.00 (89%), 402.95 (100%) $(M-1)^-$; HRMS calcd for $C_{19}H_{19}BrN_2O_3$ $(M+H)^+$ 403.0657, found 403.0654.

(*E*)-2-(4-allyl-2-methoxyphenoxy)-*N′*-(4-nitrobenzylidene)acetohydrazide (SEH05) [191, 195, 196]: White solid; Yield: 70 %; MP: 108-110 ºC; R_f: 0.80 in 60 % ethyl acetate-*n*-hexane; FTIR (KBr, *v,* cm^{-1}): 3193 (amide NH str), 3079 (aromatic CH str), 2971 (aliphatic CH_2 str), 1682 (C=O), 1637 (C=N str), 1521 (aromatic C=C str); ^{1}H NMR (500 MHz, $CDCl_3$) δ ppm 10.39 (s, 1H, amide-NH), 8.35 (s, 1H, imine-CH), 8.29 (s, 2H), 7.95 (d, *J* = 8.9 Hz, 2H), 6.94 (d, *J* = 7.9 Hz, 1H), 6.83 – 6.77 (m, 2H), 5.97 (ddt, *J* = 17.7, 9.2, 6.7 Hz, 1H), 5.13 (dq, *J* = 6.4, 1.6 Hz, 1H), 5.10 (t, *J* = 1.4 Hz, 1H), 4.73 (s, 2H, -CH_2), 3.96 (s, 3H, -OCH_3), 3.38 (d, *J* = 6.7 Hz, 2H); ^{13}C NMR (126 MHz, $CDCl_3$) δ ppm 165.59 (-C=O), 149.61, 148.81, 146.16, 145.43 (-C=N), 139.58, 137.05, 136.17, 128.34, 124.01, 121.37, 116.76, 116.20, 112.81, 70.36 (-CH_2), 55.97 (-OCH_3), 39.86; MS (ESI⁻): *m/z* = 368.10 $(M-1)^-$; HRMS calcd for $C_{19}H_{19}N_3O_5$ $(M+H)^+$ 370.1403, found 370.1392.

(*E*)-2-(4-allyl-2-methoxyphenoxy)-*N′*-(2-hydroxybenzylidene)acetohydrazide (SEH06) [195-197]: Off white solid; Yield: 51 %; MP: 90-92 ºC; R_f: 0.95 in 60 % ethyl acetate-*n*-hexane; FTIR (KBr, *v,* cm^{-1}): 3432 (aromatic OH str), 3073 (aromatic CH str), 2927 (aliphatic CH_2 str), 1677 (C=O), 1619 (C=N str), 1515 (aromatic C=C str); ^{1}H NMR (500 MHz, $CDCl_3$) δ ppm 10.99 (s, 1H, amide-NH), 10.22 (s, 1H, -OH), 8.39 (s, 1H, imine-CH), 7.38 – 7.31 (m, 1H), 7.27 – 7.22 (m, 1H), 7.03 (d, *J* = 7.0 Hz, 1H), 6.97 – 6.88 (m, 2H), 6.80 (d, *J* = 7.9 Hz, 2H), 6.03 – 5.90 (m, 1H), 5.19 – 5.06 (m, 2H), 4.71 (s, 2H, -CH_2), 3.95 (s, 3H, -OCH_3), 3.38 (d, *J* = 6.7 Hz, 2H); ^{13}C NMR (126 MHz, $CDCl_3$) δ ppm 164.63 (-C=O), 158.69, 151.62, 149.58, 145.49 (-C=N), 137.08, 136.09, 132.12, 131.05, 121.37, 119.34, 117.34, 117.24, 116.79, 116.17, 112.76, 70.36 (-CH_2), 55.94 (-OCH_3), 39.86; MS (ESI⁻): *m/z* = 339.05 $(M-1)^-$; HRMS calcd for $C_{19}H_{20}N_2O_4$ $(M+H)^+$ 341.1501, found 341.1493.

(*E*)-2-(4-allyl-2-methoxyphenoxy)-*N′*-(4-hydroxybenzylidene)acetohydrazide

(SEH07) [191, 196]: Off white solid; Yield: 69 %; MP: 74-76 ºC; R_f: 0.54 in 60 % ethyl acetate-*n*-hexane; FTIR (KBr, *v,* cm^{-1}): 3474 (aromatic OH str), 3344 (amide NH str), 3023 (aromatic CH str), 2849 (aliphatic CH_2 str), 1670 (C=O), 1636 (C=N str), 1512 (aromatic C=C str); ^{1}H NMR (500 MHz, $CDCl_3$) δ ppm 10.23 (s, 1H, amide-NH), 8.00 (s, 1H, imine-CH), 7.56 (d, *J* = 8.7 Hz, 2H), 6.94 – 6.88 (m, 3H), 6.78 (dd, *J* = 9.8, 1.9 Hz, 2H), 6.03 – 5.87 (m, 1H), 5.20 – 5.02 (m, 2H), 4.70 (s, 2H, -CH_2), 3.93 (s, 3H, -OCH_3), 3.51 (s, 1H, -OH), 3.37 (d, *J* = 6.7 Hz, 2H); ^{13}C NMR (126 MHz, $CDCl_3$) δ ppm 165.56 (-C=O), 159.44, 149.87, 149.52, 145.48 (-C=N), 137.12, 135.93, 129.78, 124.97, 121.34, 116.63, 116.14, 116.11, 112.74, 70.12 (-CH_2), 55.90 (-OCH_3), 39.85; MS (ESI^-): *m/z* = 339.05 $(M-1)^-$; HRMS calcd for $C_{19}H_{20}N_2O_4$ $(M+H)^+$ 341.1501, found 341.1495.

(*E*)-2-(4-allyl-2-methoxyphenoxy)-*N′*-(4-methoxybenzylidene)acetohydrazide

(SEH08) [195, 196]: White solid; Yield: 51 %; MP: 68-70 ºC; R_f: 0.77 in 60 % ethyl acetate-*n*-hexane; FTIR (KBr, *v,* cm^{-1}): 3191 (amide NH str), 3072 (aromatic CH str), 2957 (aliphatic CH_2 str), 1682 (C=O), 1638 (C=N str), 1515 (aromatic C=C str); ^{1}H NMR (500 MHz, $CDCl_3$) δ ppm 10.03 (s, 1H, amide-NH), 8.09 (s, 1H, imine-CH), 7.74 (d, *J* = 8.9 Hz, 2H), 6.98 – 6.90 (m, 3H), 6.79 (d, *J* = 7.9 Hz, 2H), 6.03 – 5.92 (m, 1H), 5.16 – 5.05 (m, 2H), 4.71 (s, 2H, -CH_2), 3.95 (s, 3H, -OCH_3), 3.87 (s, 3H), 3.38 (d, *J* = 6.7 Hz, 2H); ^{13}C NMR (126 MHz, $CDCl_3$) δ ppm 164.88 (-C=O), 161.74, 149.63, 148.84, 145.57 (-C=N), 137.15, 135.85, 129.52, 125.97, 121.25, 116.58, 116.12, 114.19, 112.65, 70.29 (-CH_2), 55.87 (-OCH_3), 55.40, 39.87; MS (ESI^-): *m/z* = 353.10 $(M-1)^-$,; HRMS calcd for $C_{20}H_{22}N_2O_4$ (M+H)+ 355.1658, found 355.1656.

(*E*)-2-(4-allyl-2-methoxyphenoxy)-*N′*-(2,5-dimethoxybenzylidene)acetohydrazide

(SEH09): White solid; Yield: 69 %; MP: 99-101 ºC; R_f: 0.67 in 60 % ethyl acetate-*n*-hexane; FTIR (KBr, *v,* cm^{-1}): 3192 (amide NH str), 3075 (aromatic CH str), 2940 (aliphatic

CH_2 str), 1681 (C=O), 1514 (aromatic C=C str); ^{1}H NMR (500 MHz, $CDCl_3$) δ ppm 10.27 (d, J = 17.7 Hz, 1H, amide-NH), 8.52 (s, 1H, imine-CH), 7.63 (d, J = 3.1 Hz, 1H), 7.07 – 6.65 (m, 6H), 5.97 (ddt, J = 17.0, 10.3, 6.7 Hz, 1H), 5.20 – 5.05 (m, 2H), 4.72 (s, 2H, -CH_2), 3.96 (s, 3H, -OCH_3), 3.84 (d, J = 9.1 Hz, 6H), 3.43 – 3.33 (m, 2H); ^{13}C NMR (126 MHz, $CDCl_3$) δ ppm 164.97 (-C=O), 153.87, 152.86, 149.74, 145.74, 144.93 (-C=N), 137.13, 136.02, 122.16, 121.28, 119.46, 117.20, 116.11, 112.60, 112.53, 109.97, 70.84 (-CH_2), 56.27 (-OCH_3), 56.04, 55.70, 39.88; MS (ESI^-): m/z = 383.10 $(M-1)^-$; HRMS calcd for $C_{21}H_{24}N_2O_5$ $(M+H)^+$ 385.1763, found 385.1782.

(*E*)-2-(4-allyl-2-methoxyphenoxy)-*N′*-(4-hydroxy-3-methoxybenzylidene)acetohydrazide (SEH10) [196]: Sticky off white solid; Yield: 65 %; R_f: 0.51 in 60 % ethyl acetate-*n*-hexane; FTIR (KBr, *v,* cm^{-1}): 3219 (amide NH str), 3070 (aromatic CH str), 2935 (aliphatic CH_2 str), 1675 (C=O), 1600 (C=N str), 1511 (aromatic C=C str); ^{1}H NMR (500 MHz, $CDCl_3$) δ ppm 10.08 (s, 1H, amide-NH)), 8.04 (s, 1H, imine-CH), 7.55 (s, 1H), 7.04 (d, J = 8.1 Hz, 1H), 6.92 (d, J = 8.1 Hz, 2H), 6.78 (d, J = 10.8 Hz, 2H), 6.15 (s, 1H), 6.03 – 5.86 (m, 1H), 5.11 (d, J = 16.3 Hz, 2H), 4.70 (s, 2H, -CH_2), 3.94 (s, 6H, 2x -OCH_3), 3.37 (d, J = 7.8 Hz, 2H); ^{13}C NMR (126 MHz, $CDCl_3$) δ ppm 164.98 (-C=O), 149.61, 149.41, 148.57, 147.20, 145.56 (-C=N), 137.13, 135.84, 125.84, 123.96, 121.26, 116.55, 116.11, 114.11, 112.70, 107.92, 70.21 (-CH_2), 56.24 (2x -OCH_3), 55.88, 39.85; MS (ESI^-): m/z = 369.10 $(M-1)^-$; HRMS calcd for $C_{20}H_{22}N_2O_5$ $(M+H)^+$ 371.1607, found 371.1598.

(*E*)-2-(4-allyl-2-methoxyphenoxy)-*N′*-(3-hydroxy-4-methoxybenzylidene)acetohydrazide (SEH11): Sticky off white solid; Yield: 67 %; R_f: 0.51 in 60 % ethyl acetate-*n*-hexane; FTIR (KBr, *v,* cm^{-1}): 3278 (amide NH str), 2984 (aromatic CH str), 2936 (aliphatic CH_2 str), 1664 (C=O), 1611 (C=N str), 1509 (aromatic C=C str); ^{1}H NMR (500 MHz, $CDCl_3$) δ ppm 10.12 (s, 1H, amide-NH), 8.04 (s, 1H, imine-

CH), 7.41 (s, 1H), 7.26 (d, *J* = 6.3 Hz, 1H), 6.89 (dd, *J* = 25.0, 8.2 Hz, 2H), 6.82 – 6.73 (m, 2H), 6.15 (s, 1H, -OH), 6.05 – 5.85 (m, 1H), 5.15 – 5.05 (m, 2H), 4.70 (s, 2H, -CH_2), 3.93 (d, *J* = 4.4 Hz, 6H, 2x -OCH_3), 3.37 (d, *J* = 6.9 Hz, 2H); ^{13}C NMR (126 MHz, $CDCl_3$) δ ppm 165.04 (-C=O), 149.57, 149.07, 145.97, 145.54 (-C=N), 137.15, 135.79, 126.81, 121.25, 121.00, 116.48, 116.10, 113.42, 112.65, 110.53, 70.19 (-CH_2, 55.86 (2x -OCH_3), 39.86; MS (ESI^-): *m/z* = 369.10 $(M-1)^-$; HRMS calcd for $C_{20}H_{22}N_2O_5$ $(M+H)^+$ 371.1607, found 371.1600.

***N'*-((*E*)-benzylidene)-2-(2-methoxy-4-((*E*)-prop-1-en-1-yl)phenoxy)acetohydrazide (SIEH01):** White solid; Yield: 85 %; MP: 109-111 ºC; R_f: 0.87 in 60 % ethyl acetate-*n*-hexane; FTIR (KBr, *v,* cm^{-1}): 3241 (amide NH str), 3064 (aromatic CH str), 2953 (aliphatic CH_2 str), 1672 (C=O), 1605 (C=N str), 1511 (aromatic C=C str); ^{1}H NMR (500 MHz, $CDCl_3$) δ ppm 10.09 (s, 1H, amide-NH) , 8.17 (s, 1H, imine-CH), 7.79 (d, *J* = 9.8 Hz, 2H), 7.43 (s, 3H), 7.02 – 6.82 (m, 3H), 6.37 (d, *J* = 17.4 Hz, 1H), 6.27 – 6.09 (m, 1H), 4.72 (s, 2H, -CH_2), 3.95 (d, *J* = 19.8 Hz, 3H, -OCH_3), 1.94 – 1.87 (m, 3H, -CH_3); ^{13}C NMR (126 MHz, $CDCl_3$) δ ppm 164.99 (-C=O), 149.72, 149.10, 146.10 (-C=N), 134.06, 133.33, 130.74, 130.20, 128.71, 127.89, 125.50, 119.09, 116.51, 109.41, 70.14 (-CH_2), 55.85 (-OCH_3), 18.41 (-CH_3); MS (ESI^-): m/z = 323.10 $(M-1)^-$; HRMS calcd for $C_{19}H_{20}N_2O_3$ $(M+H)^+$ 325.1552, found 325.1538.

***N'*-((*E*)-4-fluorobenzylidene)-2-(2-methoxy-4-((*E*)-prop-1-en-1-yl)phenoxy)acetohydrazide (SIEH02):** White solid; Yield: 90 %; MP: 130-132 ºC; R_f: 0.84 in 60 % ethyl acetate-*n*-hexane; FTIR (KBr, *v,* cm^{-1}): 3191 (amide NH str), 2984 (aromatic CH str), 2936 (aliphatic CH_2 str), 1664 (C=O), 1611 (C=N str), 1509 (aromatic C=C str), 1145 (aromatic C-F str); ^{1}H NMR (500 MHz, $CDCl_3$) δ ppm 10.10 (s, 1H, amide-NH), 8.16 (s, 1H, imine-CH), 7.78 (dd, *J* = 8.9, 5.4 Hz, 2H), 7.11 (t, *J* = 8.6 Hz, 2H), 6.93 (d, *J* = 19.8 Hz, 3H), 6.36 (d, *J* = 15.7 Hz, 1H), 6.25 – 6.09 (m, 1H), 4.71 (s, 2H, -CH_2),

3.96 (s, 3H, -OCH_3), 1.89 (d, J = 8.9 Hz, 3H, -CH_3); ^{13}C NMR (126 MHz, $CDCl_3$) δ ppm 165.03 (-C=O), 163.25, 149.68, 147.87, 146.05 (-C=N), 134.06, 130.17, 129.81, 129.74, 125.53, 124.36, 119.10, 116.44, 116.01, 115.84, 109.42, 70.06 (-CH_2), 55.86 (-OCH_3), 18.41 (-CH_3); MS (ESI^-): 341.10 $(M-1)^-$; HRMS calcd for $C_{19}H_{19}FN_2O_3$ $(M+H)^+$ 343.1458, found 343.1445.

***N′*-((*E*)-4-chlorobenzylidene)-2-(2-methoxy-4-((*E*)-prop-1-en-1-yl)phenoxy)acetohydrazide (SIEH03):** White solid; Yield: 70 %; MP: 130-132 ºC; R_f: 0.87 in 60 % ethyl acetate-*n*-hexane; FTIR (KBr, *v,* cm^{-1}): 3186 (amide NH str), 3085 (aromatic CH str), 2958 (aliphatic CH_2 str), 1684 (C=O), 1611 (C=N str), 1512 (aromatic C=C str), 1035 (aromatic C-Cl str); ^{1}H NMR (500 MHz, $CDCl_3$) δ ppm 10.14 (s, 1H, amide-NH), 8.15 (s, 1H, imine-CH), 7.72 (d, J = 8.5 Hz, 2H), 7.39 (d, J = 8.5 Hz, 2H), 6.92 (d, J = 20.3 Hz, 3H), 6.41 – 6.29 (m, 1H), 6.23 – 6.08 (m, 1H), 4.71 (s, 2H, -CH_2), 3.93 (d, J = 20.8 Hz, 3H, -OCH_3), 1.97 – 1.83 (m, 3H, -CH_3); ^{13}C NMR (126 MHz, $CDCl_3$) δ ppm 165.10 (-C=O), 149.69, 147.75, 146.05 (-C=N), 136.65, 134.08, 131.91, 130.17, 129.03, 128.99, 125.54, 124.39, 119.10, 116.47, 109.43, 70.09 (-CH_2), 55.86 (-OCH_3), 18.42 (-CH_3); MS (ESI^-): *m/z* = 357.05 $(M-1)^-$; HRMS calcd for $C_{19}H_{19}ClN_2O_3$ $(M+H)^+$ 359.1162, found 359.1141.

***N′*-((*E*)-4-bromobenzylidene)-2-(2-methoxy-4-((*E*)-prop-1-en-1-yl)phenoxy)acetohydrazide (SIEH04):** White solid; Yield: 83 %; MP: 135-137 ºC; R_f: 0.89 in 60 % ethyl acetate-*n*-hexane; FTIR (KBr, *v,* cm^{-1}): 3189 (amide NH str), 3087 (aromatic CH str), 2957 (aliphatic CH_2 str), 1684 (C=O), 1609 (C=N str), 1513 (aromatic C=C str), 1067 (aromatic C-Br str); ^{1}H NMR (500 MHz, $CDCl_3$) δ ppm 10.11 (s, 1H, amide-NH), 8.15 (s, 1H, imine-CH), 7.66 (d, J = 8.5 Hz, 2H), 7.56 (d, J = 8.5 Hz, 2H), 6.93 (d, J = 19.5 Hz, 3H), 6.37 (d, J = 17.4 Hz, 1H), 6.18 (dd, J = 15.7, 6.6 Hz, 1H), 4.72 (s, 2H, -CH_2), 3.96 (s, 3H, -OCH_3), 1.90 (d, J = 6.6 Hz, 3H, -CH_3); ^{13}C NMR (126 MHz, $CDCl_3$) δ

ppm 165.08 (-C=O), 149.71, 147.81, 146.05 (-C=N), 134.13, 132.36, 131.99, 130.17, 129.20, 125.56, 125.07, 119.11, 116.53, 109.47, 70.14 ($-CH_2$), 55.89 ($-OCH_3$), 18.40 ($-CH_3$); MS (ESI^-): *m/z* = 401.00 (98%), 403.00 (100%) $(M-1)^-$; HRMS calcd for $C_{19}H_{19}BrN_2O_3$ $(M+H)^+$ 403.0657, found 403.0654.

2-(2-Methoxy-4-((*E*)-prop-1-en-1-yl)phenoxy)-*N′*-((*E*)-4-nitrobenzylidene)acetohydrazide (SIEH05): White solid; Yield: 76 %; MP: 147-149 ºC; R_f: 0.79 in 60 % ethyl acetate-*n*-hexane; FTIR (KBr, *v,* cm^{-1}): 3193 (amide NH str), 3076 (aromatic CH str), 2962 (aliphatic CH_2 str), 1686 (C=O), 1615 (C=N str), 1523 (aromatic C=C str); ^1H NMR (500 MHz, $CDCl_3$) δ ppm 10.35 (s, 1H, amide-NH), 8.35 (s, 1H, imine-CH), 8.28 (d, *J* = 8.9 Hz, 2H), 7.95 (d, *J* = 9.0 Hz, 2H), 6.94 (d, *J* = 18.6 Hz, 3H), 6.37 (d, *J* = 17.4 Hz, 1H), 6.19 (dt, *J* = 15.7, 6.7 Hz, 1H), 4.73 (s, 2H, $-CH_2$), 3.97 (s, 3H, $-OCH_3$), 1.90 (d, *J* = 5.0 Hz, 3H, $-CH_3$); ^{13}C NMR (126 MHz, $CDCl_3$) δ ppm 165.48 (-C=O), 149.65, 148.81, 146.21, 145.94 (-C=N), 139.55, 134.25, 130.11, 128.35, 125.69, 124.01, 119.16, 116.55, 109.53, 70.12 ($-CH_2$), 55.94 ($-OCH_3$), 18.42 ($-CH_3$); MS (ESI^-): *m/z* = 368.10 $(M-1)^-$; HRMS calcd for $C_{19}H_{19}N_3O_5$ $(M+H)^+$ 370.1403, found 370.1394.

***N′*-((*E*)-2-hydroxybenzylidene)-2-(2-methoxy-4-((*E*)-prop-1-en-1-yl)phenoxy)acetohydrazide (SIEH06):** Off white solid; Yield: 79 %; MP: 122-124 ºC; R_f: 0. 97 in 60 % ethyl acetate-*n*-hexane; FTIR (KBr, *v,* cm^{-1}): 3417 (aromatic OH str), 3187 (amide NH str), 3093 (aromatic CH str), 2957 (aliphatic CH_2 str), 1675 (C=O), 1618 (C=N str), 1515 (aromatic C=C str); ^1H NMR (500 MHz, $CDCl_3$) δ ppm 11.00 (s, 1H, amide-NH), 10.20 (s, 1H, -OH), 8.38 (s, 1H, imine-CH), 7.37 – 7.29 (m, 1H), 7.26 – 7.21 (m, 1H), 7.03 (d, *J* = 7.2 Hz, 1H), 6.98 – 6.85 (m, 4H), 6.36 (d, *J* = 17.4 Hz, 1H), 6.18 (dd, *J* = 15.6, 6.6 Hz, 1H), 4.70 (s, 2H, $-CH_2$), 3.96 (s, 3H, $-OCH_3$), 1.90 (d, *J* = 6.6 Hz, 3H, $-CH_3$); ^{13}C NMR (126 MHz, $CDCl_3$) δ ppm 164.53 (-C=O), 158.68, 151.64, 149.63, 146.01 (-C=N),

134.18, 132.13, 131.07, 130.15, 125.61, 119.34, 119.16, 117.33, 117.23, 116.57, 109.48, 70.10 (-CH_2), 55.89 (-OCH_3), 18.42 (-CH_3); MS (ESI^-): *m/z* = 339.10 $(M-1)^-$.

***N′*-((*E*)-4-hydroxybenzylidene)-2-(2-methoxy-4-((*E*)-prop-1-en-1-yl)phenoxy)acetohydrazide (SIEH07):** Off white solid; Yield: 81 %; MP: 151-153 ºC; R_f: 0. 50 in 60 % ethyl acetate-*n*-hexane; FTIR (KBr, *v,* cm^{-1}): 3276 (amide NH str), 3017 (aromatic CH str), 2929 (aliphatic CH_2 str), 1668 (C=O), 1608 (C=N str), 1510 (aromatic C=C str); ^1H NMR (500 MHz, $CDCl_3$) δ ppm 10.09 (s, 1H, amide-NH), 8.03 (s, 1H, imine-CH), 7.62 (d, *J* = 8.7 Hz, 2H), 7.05 – 6.80 (m, 5H), 6.48 – 6.30 (m, 1H), 6.24 – 6.15 (m, 1H), 5.32 (s, 1H, -OH), 4.72 (s, 2H, -CH_2), 3.96 (s, 3H, -OCH_3), 1.90 (d, *J* = 8.4 Hz, 3H, -CH_3); ^{13}C NMR (126 MHz, $CDCl_3$) δ ppm 165.19 (-C=O), 149.65, 149.47, 146.07 (-C=N), 134.09, 130.18, 129.78, 125.54, 125.36, 119.14, 116.53, 116.02, 109.45, 70.05 (-CH_2), 55.86 (-OCH_3), 18.41 (-CH_3); MS (ESI^-): *m/z* = 339.05 $(M-1)^-$.

2-(2-Methoxy-4-((*E*)-prop-1-en-1-yl)phenoxy)-*N′*-((*E*)-4-methoxybenzylidene)acetohydrazide (SIEH08): White solid; Yield: 66 %; MP: 126-128 ºC; R_f: 0.75 in 60 % ethyl acetate-*n*-hexane; FTIR (KBr, *v,* cm^{-1}): 3191 (amide NH str), 3092 (aromatic CH str), 2955 (aliphatic CH_2 str), 1682 (C=O), 1605 (C=N str), 1515 (aromatic C=C str); ^1H NMR (500 MHz, $CDCl_3$) δ ppm 10.03 (s, 1H, amide-NH), 8.08 (s, 1H, imine-CH), 7.79 – 7.66 (m, 2H), 6.97 – 6.87 (m, 5H), 6.35 (d, *J* = 17.4 Hz, 1H), 6.21 – 6.08 (m, 1H), 4.70 (s, 2H, -CH_2), 3.94 (s, 3H, -OCH_3), 3.85 (s, 3H), 1.89 (d, *J* = 6.6 Hz, 3H, -CH_3); ^{13}C NMR (126 MHz, $CDCl_3$) δ ppm 164.80 (-C=O), 161.73, 149.66, 148.95, 146.12 (-C=N), 133.92, 130.21, 129.52, 125.41, 119.06, 116.32, 109.37, 70.00 (-CH_2), 55.82 (-OCH_3), 55.39, 18.41 (-CH_3); MS (ESI^-): *m/z* = 353.10 $(M-1)^-$.

***N′*-((*E*)-2,5-dimethoxybenzylidene)-2-(2-methoxy-4-((*E*)-prop-1-en-1-yl)phenoxy)acetohydrazide (SIEH09):** White solid; Yield: 78 %; MP: 111-113 ºC; R_f:

0.82 in 60 % ethyl acetate-*n*-hexane; FTIR (KBr, *v,* cm^{-1}): 3332 (amide NH str), 3079 (aromatic CH str), 2914 (aliphatic CH_2 str), 1695 (C=O), 1513 (aromatic C=C str); ^{1}H NMR (500 MHz, $CDCl_3$) δ ppm 10.22 (s, 1H, amide-NH), 8.52 (s, 1H, imine-CH), 7.63 (d, J = 3.2 Hz, 1H), 6.99 – 6.94 (m, 2H), 6.92 (d, J = 4.6 Hz, 2H), 6.87 (d, J = 9.0 Hz, 1H), 6.36 (d, J = 15.7 Hz, 1H), 6.18 (dd, J = 15.7, 6.6 Hz, 1H), 4.73 (s, 2H, -CH_2), 3.98 (s, 3H, -OCH_3), 3.84 (d, J = 8.2 Hz, 6H), 1.90 (d, J = 6.6 Hz, 3H, -CH_3); ^{13}C NMR (126 MHz, $CDCl_3$) δ ppm 164.89 (-C=O), 153.84, 152.86, 149.75, 146.24, 145.00 (-C=N), 134.13, 130.21, 125.52, 122.08, 119.50, 119.09, 116.97, 112.58, 109.91, 109.24, 70.57 (-CH_2), 56.26 (-OCH_3), 56.04, 55.67, 18.43 (-CH_3); MS (ESI^-): m/z = 383.15 $(M-1)^-$.

***N′*-((*E*)-4-hydroxy-3-methoxybenzylidene)-2-(2-methoxy-4-((*E*)-prop-1-en-1-yl)phenoxy)acetohydrazide (SIEH10):** White solid; Yield: 70 %; MP: 90-92 ºC; R_f: 0.50 in 60 % ethyl acetate-*n*-hexane; FTIR (KBr, *v,* cm^{-1}): 3224 (amide NH str), 3067 (aromatic CH str), 2927 (aliphatic CH_2 str), 1675 (C=O), 1600 (C=N str), 1511 (aromatic C=C str); ^{1}H NMR (500 MHz, $CDCl_3$) δ ppm 10.01 (s, 1H, amide-NH), 8.05 (s, 1H, imine-CH), 7.55 (s, 1H), 7.05 (dd, J = 8.0, 1.9 Hz, 1H), 6.98 – 6.88 (m, 4H), 6.36 (d, J = 15.7 Hz, 1H), 6.26 – 6.12 (m, 1H), 6.06 (s, 1H, -OH), 4.71 (s, 2H, -CH_2), 3.99 – 3.94 (m, 6H, 2x -OCH_3), 1.90 (d, J = 8.2 Hz, 3H, -CH_3); ^{13}C NMR (126 MHz, $CDCl_3$) δ ppm 164.83 (-C=O), 149.69, 149.44, 148.55, 147.16, 146.11 (-C=N), 134.01, 130.20, 125.82, 125.47, 124.00, 121.11, 119.08, 116.40, 114.08, 112.61, 109.42, 107.89, 70.05 (-CH_2), 56.28 (-OCH_3), 55.85, 18.40 (-CH_3); MS (ESI^-): m/z = 369.10 $(M-1)^-$.

***N′*-((*E*)-3-hydroxy-4-methoxybenzylidene)-2-(2-methoxy-4-((*E*)-prop-1-en-1-yl)phenoxy)acetohydrazide (SIEH11):** White solid; Yield: 50 %; MP: 138-140 ºC; R_f: 0.50 in 60 % ethyl acetate-*n*-hexane; FTIR (KBr, *v,* cm^{-1}): 3277 (amide NH str), 2988 (aromatic CH str), 2937 (aliphatic CH_2 str), 1664 (C=O), 1612 (C=N str), 1510 (aromatic C=C str); ^{1}H NMR (500 MHz, $CDCl_3$) δ ppm 10.02 (s, 1H, amide-NH), 8.05 (s, 1H, imine-

CH), 7.40 (s, 1H), 7.01 – 6.74 (m, 4H), 6.37 (d, J = 17.4 Hz, 1H), 6.25 – 6.08 (m, 1H), 5.87 (s, 1H, -OH), 4.71 (s, 2H, -CH_2), 4.04 – 3.82 (m, 6H, 2x -OCH_3), 1.90 (d, J = 6.6 Hz, 3H, -CH_3); ^{13}C NMR (126 MHz, $CDCl_3$) δ ppm 164.83 (-C=O), 149.67, 149.04, 148.94, 146.11, 145.90 (-C=N), 133.97, 130.21, 126.83, 125.45, 120.95, 119.07, 116.39, 113.44, 110.48, 109.37, 70.05 (-CH_2), 56.01 (-OCH_3), 55.83, 18.41 (-CH_3); MS (ESI^-): m/z = 369.10 $(M-1)^-$; HPLC purity: 99.98 %.

4.4.2. Biological Studies

4.4.2.1. *In vitro* studies

The enzyme inhibition screening study of compounds **SEH01-SEH11** and **SIEH01-SIEH11** was performed against MAOs (MAO-A and MAO-B) and ChEs (AChE and BChE) using peroxidase-linked colorimetric assay method and Ellman's UV based method, respectively. The obtained results of enzyme inhibition studies are given in the **Table 4.2**. High potency (less than 2 micromolar) was observed with all compounds against all three targets.

Table 4.2. *In vitro* enzyme inhibition results of compounds **SEH01-SEH11** and **SIEH01-SIEH11**

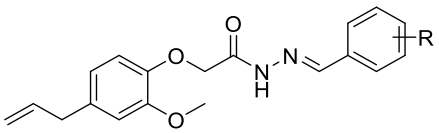

SEH01-SEH11

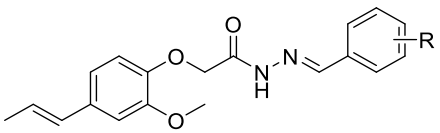

SIEH01-SIEH11

Compd. code	R	MAO-A IC_{50} [µM][a]	MAO-B IC_{50} [µM][a]	S.I.[b]	AChE IC_{50} [µM][a]	BChE IC_{50} [µM][a]
SEH01	H	1.802 ± 0.026	2.002 ± 0.014	0.90	1.162 ± 0.053	NT
SEH02	4-F	1.056 ± 0.094	1.308 ± 0.093	0.81	1.226 ± 0.033	NT
SEH03	4-Cl	0.528 ± 0.091	0.857 ± 0.036	0.62	1.254 ± 0.034	NT
SEH04	4-Br	1.374 ± 0.187	0.107 ± 0.025	12.84	1.204 ± 0.043	NT
SEH05	4-NO_2	1.191 ± 0.096	1.827 ± 0.377	0.65	1.079 ± 0.104	NT
SEH06	2-OH	0.053 ± 0.012	0.543 ± 0.054	0.10	1.270 ± 0.001	NT
SEH07	4-OH	0.870 ± 0.123	0.167 ± 0.003	5.21	1.226 ± 0.020	NT
SEH08	4-OCH_3	1.054 ± 0.011	0.495 ± 0.073	2.13	1.209 ± 0.029	NT
SEH09	2,5-di-OCH_3	0.326 ± 0.081	0.109 ± 0.001	2.99	1.192 ± 0.001	NT

SEH10	3-OCH_3, 4-OH	1.300 ± 0.219	0.979 ± 0.126	1.33	1.223 ± 0.013	NT
SEH11	3-OH, 4-OCH_3	1.132 ± 0.014	0.051 ± 0.001	22.19	1.183 ± 0.083	NT
SIEH01	H	0.544 ± 0.018	0.160 ± 0.010	3.40	1.229 ± 0.048	NT
SIEH02	4-F	0.558 ± 0.046	1.123 ± 0.054	0.50	1.243 ± 0.010	NT
SIEH03	4-Cl	1.836 ± 0.020	0.676 ± 0.033	2.71	1.210 ± 0.092	NT
SIEH04	4-Br	1.493 ± 0.057	0.054 ± 0.012	27.65	1.329 ± 0.006	NT
SIEH05	4-NO_2	1.188 ± 0.126	0.990 ± 0.010	1.20	1.397 ± 0.029	NT
SIEH06	2-OH	0.144 ± 0.024	0.024 ± 0.011	6.00	1.283 ± 0.025	NT
SIEH07	4-OH	1.490 ± 0.197	0.482 ± 0.044	3.09	1.308 ± 0.005	NT
SIEH08	4-OCH_3	1.391 ± 0.132	0.114 ± 0.014	12.20	1.310 ± 0.039	NT
SIEH09	2,5-di-OCH_3	1.810 ± 0.058	0.184 ± 0.025	9.83	1.220 ± 0.021	NT
SIEH10	3-OCH_3, 4-OH	1.901 ± 0.102	0.034 ± 0.002	55.91	1.316 ± 0.013	9.827 ± 0.109
SIEH11	3-OH, 4-OCH_3	0.289 ± 0.059	0.366 ± 0.076	0.79	1.339 ± 0.019	NT
CLO	-	0.096 ± 0.003	-	-	-	-
SEL	-	-	0.021 ± 0.002	-	-	-
PCPA	-	0.141 ± 0.002	0.201 ± 0.001	0.70	-	-
DPZ	-	-	-	-	0.073 ± 0.001	1.751 ± 0.120

[a] Values are the mean of IC_{50} ± SEM of n = 2 experiments in triplicate (MAO-A, MAO-B and AChE); [b] Selectivity index: ratio of experimental IC_{50}(MAO-A)/IC_{50}(MAO-B); CLO = Clorgyline, SEL = Selegiline; PCPA = Tranylcypromine, DPZ = Donepezil; NT = Not tested.

4.4.2.1.1. *In vitro* MAO inhibition studies

Enzyme inhibition studies of compounds **SEH01-SEH11** and **SIEH01-SIEH11** were performed against MAO-A and obtained IC_{50} results were in the range of micromolar to nanomolar concentration (compound **SIEH10,** 1.901 ± 0.102 μM, to compound **SEH06,** 0.053 ± 0.012 μM,) and are listed in **Table 4.2**. Among all the tested compounds, compound **SEH06** emerged as the most potent MAO-A inhibitor with an IC_{50} value of 0.053 ± 0.012 μM. The obtained IC_{50} values of compounds **SEH01-SEH11** and **SIEH01-SIEH11** against MAO-B assay ranges from micromolar to nanomolar (2.002 ± 0.014 μM, compound **SEH01** to 0.024 ± 0.011 μM, compound **SIEH06**) concentration and are listed in **Table 4.2**. Compound **SIEH06** emerged as the most potent MAO-B inhibitor among all the tested compounds and lies near the IC_{50} value of standard MAO-B inhibitor selegiline.

The inclusion of mono- or di substituents on the phenyl ring at the carbimino terminal of eugenol/isoeugenol-derived carbohydrazone resulted in variable activity profiles against MAOs and the SAR against each enzyme is discussed below.

SAR of MAO-A inhibition

- The eugenol analog bearing 2-hydroxy substitution at the N-terminal aryl ring was identified as the most potent MAO-A inhibitor having IC_{50} value of 0.053 ± 0.012 µM and it was more potent than reference inhibitor clorgyline.
- Substitution of the mono-fluoro group (compound **SEH02**) at terminal aryl ring increased the activity of eugenol analog but did not have much effect on the isoeugenol analog (compound **SIEH02**).
- The inclusion of 4-chloro group on the aryl ring enhanced the activity (~3-fold) of eugenol analog (compound **SEH03**) while it reduced the activity (3-fold) of isoeugenol analog (compound **SIEH03**).
- The substitution with a 4-bromo group (compound **SEH04**) led to a moderate increase in MAO-A inhibition of eugenol analog but reduced the activity of isoeugenol analog (~3-fold, compound **SIEH04**).
- The introduction of the 4-nitro group (compound **SEH05**) moderately enhanced the activity of eugenol analog while decreasing the activity of isoeugenol analog (compound **SIEH05**).
- Analog of both isomers with 4-hydroxyl and 4-methoxyl substitution resulted in a drastic reduction in MAO-A inhibition activity (compare compounds **SEH07**, **SEH08**, and **SIEH07**, **SIEH08** with compound **SEH06** and **SIEH06**, respectively) compared to 2-hydroxy analog.
- Substitution with the 2,5-dimethoxy group decreased the activity of both isomeric analogs (compounds **SEH09** and **SIEH09**) compared to mono methoxy substitution (compounds **SEH08** and **SIEH08**).

- Di-substitution with 3-methoxy-4-hydroxy group resulted in decreased MAO-A inhibitory activity of isomeric analogs (compounds **SEH10** and **SIEH10**) compared to the respective mono-substituted analogs.
- Di-substitution with the 3-hydroxy-4-methoxy group resulted in no change in the activity of eugenol analog (compound **SEH11**) but enhanced activity (6.5-fold) of isoeugenol analog (compound **SIEH11**) compared to compound **SIEH10**.

SAR of MAO-B inhibition

- Analog of isoeugenol with 2-hydroxy substitution (compound **SIEH06**) emerged as the most potent MAO-B inhibitor with an IC_{50} value of 0.024 ± 0.011 µM, (compound **SIEH06**) whereas the 2-hydroxy analog of eugenol (compound **SEH10**) showed superior activity (4-fold) compared to the unsubstituted analog (compound **SEH01**).
- The introduction of the 4-fluoro group (compound **SEH02**) caused improvement in the activity of eugenol analog but reduced the activity of isoeugenol by ~7-fold (compound **SIEH02**) compared to the unsubstituted analog.
- Replacement of 4-fluoro group with chloro group enhanced activity of eugenol analog by ~1.5-fold and ~2-fold of isoeugenol analog (compare compound **SIEH03** with **SIEH02**).
- Substitution with the 4-bromo group increased the activity of both analogs (compounds **SEH04** and **SIEH04**) by ~8-fold and ~12-fold, respectively while the introduction of the 4-nitro group drastically reduced MAO-B inhibition potential of resulting analogs (compounds **SEH05** and **SIEH05**).
- Hydroxyl group substituted at 2^{nd} and 4^{th} position favored the MAO-B inhibitory activity of eugenol analog (compounds **SEH06** and **SEH07**) while on isoeugenol

analog with 2-hydroxy group resulted in ~6-fold increase of activity but 4-hydroxy substitution caused ~3.6-fold reduction in activity (compounds **SIEH06** and **SIEH07**) compared to the unsubstituted analog.

- Altering lipophilicity at the 4th position of the N-terminal aryl ring (replacement of 4-hydroxyl with 4-methoxyl group) diminished the activity of eugenol analog but moderately increased activity of isoeugenol analog (compounds **SEH08** and **SIEH08**).
- Di-methyl substitution at the 2nd and 5th positions enhanced the MAO-B inhibition of the eugenol analog but reduced the activity of the isoeugenol analog (compounds **SEH09** and **SIEH09**).
- Di-substitution with 3-methoxyl and 4-hydroxyl favored and increased ~5-fold MAO-B inhibitory activity of isoeugenol analog (compound **SIEH10**) compared to di-methoxy substituted but decreased activity of eugenol analog by ~9-fold (compound **SEH10**).
- Di-substitution with 3-hydroxyl and 4-methoxyl favored activity (compound **SEH11**) over di-methyl analog but reduced the activity of isoeugenol analog (compound **SIEH11**).
- Compound **SIEH10** has the highest selectivity (55-fold) towards MAO-B over MAO-A.

4.4.2.1.2. *In vitro* ChEs inhibition assay

In vitro enzyme screening of compounds **SEH01-SEH11** and **SIEH01-SIEH11** was performed against *ee*AChE while compound **SIEH10** was assayed against *eq*BChE to evaluate the ChE selectivity of the compound. Obtained results of AChE ranges in micromolar (1.397 ± 0.029 μM compound **SIEH05** to 1.079 ± 0.104 μM, compound **SEH05**) concentration are given in **Table 4.2**. Compound **SEH05**, emerged as the most

potent AChE inhibitor with an IC_{50} value of 1.079 ± 0.104 μM among all tested compounds. The obtained BChE inhibition data (IC_{50} = 9.827 ± 0.109 μM) of compound **SIEH10** shows selectivity towards AChE.

The obtained narrow IC_{50} values suggest that the attempted structural variation did not influence the AChE inhibitory activity of the isomeric eugenol analogs.

SAR of dual MAO-AChE inhibition

- Compounds **SEH01-SEH11** and **SIEH01-SIEH11** were screened against MAO-A, MAO-B, and AChE to evaluate their inhibitory potency while compound **SIEH10** was evaluated against BChE to determine the selectivity of the compound towards AChE. The resulting IC_{50} values range in micromolar to nanomolar concentration for MAO-A and MAO-B while for ChEs in micromolar concentration and are listed in **Table 4.2.**
- Substitution of the 4-fluoro group in eugenol analog (compound **SEH02**) increased the MAO-A and MAO-B inhibitory activity but reduced the AChE inhibition whereas in isoeugenol analog, it decreased the activity against all targets compared to unsubstituted analogs.
- Introduction of the 4-chloro group (compound **SEH03**) enhanced MAO-A and MAO-B inhibitory activity but decreased the AChE inhibitory potency of eugenol analog; whereas 4-chloro substitution reduced MAO-A inhibition (~3-fold) of isoeugenol analog but increased MAO-B and AChE inhibition compared to fluoro analog (compound **SIEH02**).
- Replacement of 4-chloro with 4-bromo group diminished MAO-A inhibition of eugenol analog and AChE inhibition of isoeugenol analog while enhanced inhibition for other targets (compound **SEH04** and **SIEH04**).

4.4.2.1.3. Enzyme kinetics and reversibility

A compound with a dual inhibitory profile and highest selectivity was chosen for enzyme kinetics and time-dependent reversibility study against MAO-B and AChE enzymes. To understand the type of enzyme inhibition, a double reciprocal (Lineweaver-Burk) plot was constructed using variable concentrations of substrate and inhibitor. The obtained double reciprocal plot of compound **SIEH10** indicates the competitive inhibitor nature of the compounds against MAO-B (**Figure 4.4A**) while mixed-type reversible inhibition towards AChE (**Figure 4.4C**). Time-dependent reversibility study of compound **SIEH10** with MAO-B and AChE enzymes revealed that the compound was an irreversible inhibitor against MAO-B while reversible inhibitor towards AChE for at least 60 minutes (**Figure 4.4B** & **4.4D**).

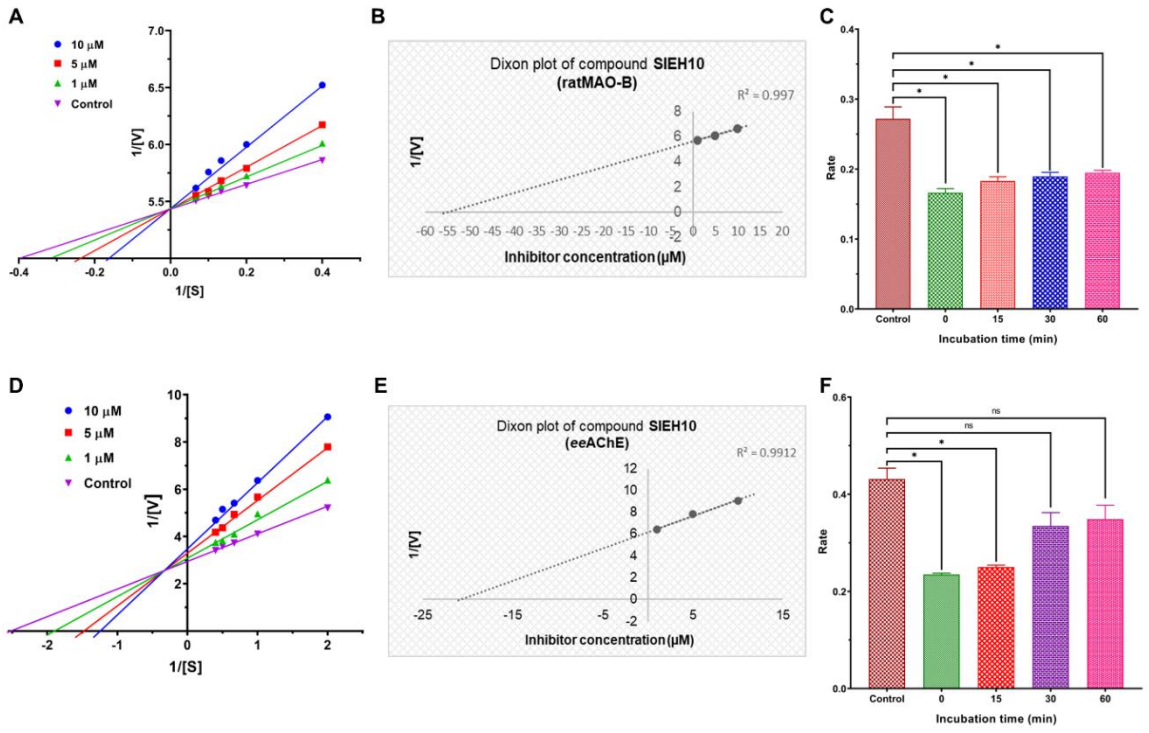

Figure 4.4. Enzyme kinetics and time-dependent reversibility data of compound **SIEH10**; A) Enzyme kinetics graph of compound **SIEH10** with ratMAO-B; B) Dixon plot of compound **SIEH10** with ratMAO-B; C) Time-dependent reversibility profile of compound **SIEH10** with ratMAO-B; D) Enzyme kinetics graph of compound **SIEH10** with *ee*AChE; E) Dixon plot of compound **SIEH10** with *ee*AChE; F) Time-dependent reversibility profile of compound **SIEH10** with *ee*AChE.

4.4.2.1.4. *In vitro* antioxidant assay

Oxidative stress, one of the leading causes of neuronal and cellular damage is propagated due to impaired antioxidant system as well as increased events of cellular insult and damage. A compromised antioxidant system leads to an increased level of reactive oxygen species (ROS) and a reduced level of superoxide dismutase (a natural free radical scavenging agent). Hyperactivity of MAO-B produces excess hydrogen peroxide which causes cellular damage. Scavenging of free radicals using antioxidant molecules can reduce the level of free radicals in the cell and subsequent cellular damage. The % free radical scavenging activity of screened molecules is presented in **Figure 4.5**. Compound **SIEH10** emerged as the most potent molecule with ~75 % FRS activity (EC_{50} = 89.37 ± 2.209). The antioxidant potency of the compound may be due to the presence of 3-methoxy and 4-hydroxy group (vanillin) which are known to efficiently scavenge free radicals.

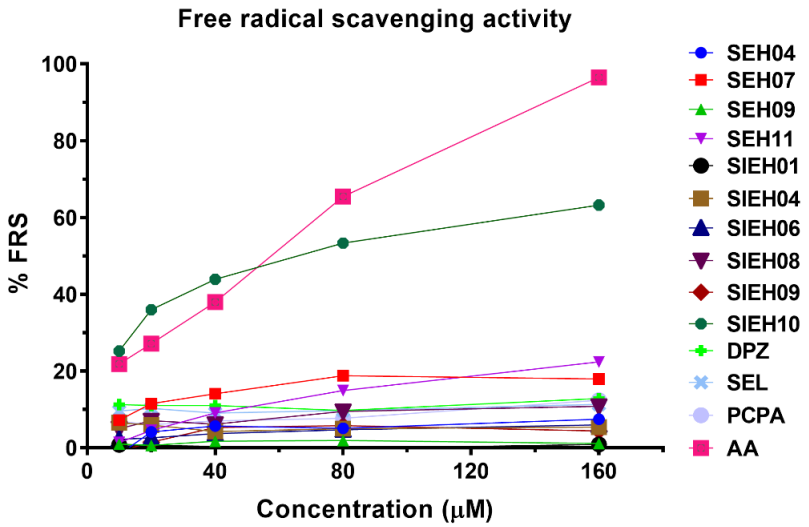

Figure 4.5. Antioxidant (free radical scavenging) activity of selected compounds; DPZ = Donepezil, SEL = Selegiline, PCPA = Tranylcypromine, and AA = Ascorbic acid.

As can be seen from **Table 4.3** most of the compounds have weak antioxidant activity but compound **SIEH10** displayed the highest free radical scavenging of about 75 % and EC_{50} values of 89 μM which is near to reference compound ascorbic acid (EC_{50} = 62 μM).

Table 4.3. Percent FRS and EC_{50} values of selected compounds

Compound code	Antioxidant activity by DPPH assay

	% FRS[a]	EC_{50} (μM)
SEH04	15.00 ± 0.976	697.84 ± 10.343
SEH07	22.48 ± 0.080	641.97 ± 9.358
SEH09	3.80 ± 0.032	3026.00 ± 27.873
SEH11	28.99 ± 0.986	356.76 ± 11.545
SIEH01	3.39 ± 0.072	3665.21 ± 7.522
SIEH04	7.67 ± 0.006	2157.61 ± 39.290
SIEH06	7.03 ± 0.168	1954.05 ± 6.864
SIEH08	13.23 ± 0.081	1149.03 ± 11.377
SIEH09	11.93 ± 0.369	1087.18 ± 6.358
SIEH10	74.98 ± 0.543	89.37 ± 2.209
Donepezil	11.70 ± 0.810	2174.10 ± 79.560
Selegiline	11.26 ± 0.150	1613.30 ± 46.040
Tranylcypromine	12.68 ± 0.736	1324.80 ± 40.540
Ascorbic acid[b]	66.89 ± 2.070	62.14 ± 0.360

[a] % FRS in 200 μM concentration; [b] % FRS in 100 μM concentration.

4.4.2.1.5. *In vitro* metal chelation assay

Metal ions (Fe, Cu, and Zn) are trace elements that play a significant role in the homeostasis and functioning of crucial enzymes. For instance, iron and copper act as redox-active metals while zinc is a Lewis acid. The impaired functioning of metal ions is one of the major causes responsible for malfunctioning and misfolding of newly synthesized proteins. Misfolding and defects in the functional proteins lead to severe illnesses such as neurodegeneration. The excess level of iron increases the catalysis of the Fenton reaction which further enhances the production of hydroxyl radicals. These excess free radicals can be removed by using suitable chelators. The iron chelation study was carried out for respective leads of MAO-B (compounds **SIEH06** and **SIEH10**) and AChE (compound **SEH05**). Compound **SIEH06** clearly shows a shift of absorption maxima (**Figure 4.6B**) which indicates the chelation of iron ions. Surprisingly, compounds **SEH05** and **SIEH10** show very little or negligible shift in the absorption maxima of the resulting mixture (**Figure 4.6A and 4.6C**).

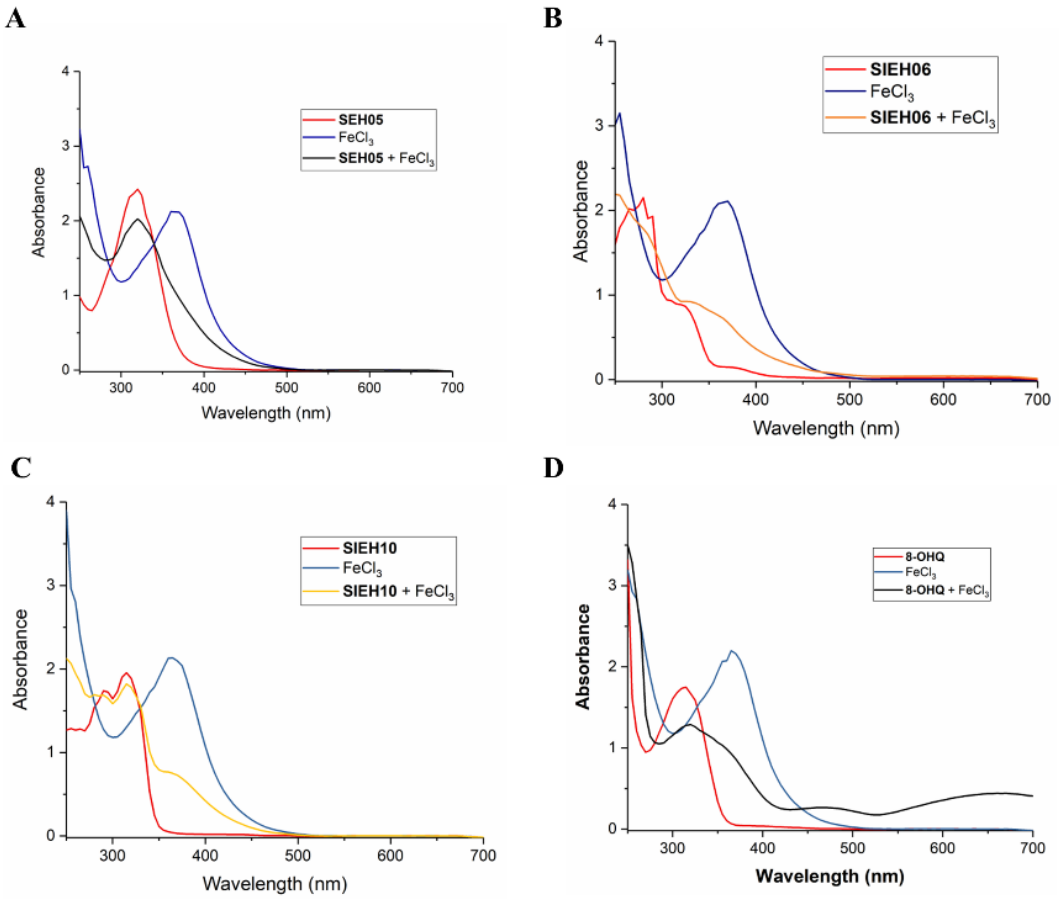

Figure 4.6. UV absorption spectra of compounds **SEH05**, **SIEH06** and **SIEH10** with and without $FeCl_3$; A) Compound **SEH05**; B) Compound **SIEH06**; C) Compound **SIEH10** and; D) **8-OHQ** (8-Hydroxyquinoline) as reference iron chelator.

4.4.2.1.6. *In vitro* blood-brain-barrier permeation assay

A new chemical entity designed to target the brain needs to reach its destiny without putting in any extra effort. The brain accessibility of a new molecule is validated using a passive permeation-based PAMPA-BBB assay. Compound **SIEH10** was evaluated for its *in vitro* blood-brain-barrier permeability using selegiline and donepezil as reference drugs while imipramine and tenoxicam were used as permeability controls, respectively. Compound **SIEH10** displayed an effective permeability (P_e) of 4.796 ± 0.075 $\times 10^{-6}$ cm/s after 18 h of incubation. **Table 4.4** shows the effective permeability (P_e) of test and reference compounds. As reported by Di et al., the molecule with $P_e > 4.0 \times 10^{-6}$ cm/s is considered CNS+ while the molecule with $P_e < 2.0 \times 10^{-6}$ cm/s is considered CNS-. Whereas a molecule

with $P_e < 4.0 \times 10^{-6}$ cm/s and $P_e > 2.0 \times 10^{-6}$ cm/s is considered as CNS is considered as CNS±. Thus, compound **SIEH10** falls under the class of CNS+ molecules and has the potential to passively permeate the BBB.

Table 4.4. PAMPA-BBB assay result of compound **SIEH10**

Compound ID	P_e ($\times 10^{-6}$ cm/s)[a]	Reference P_e ($\times 10^{-6}$ cm/s)[b]	*In Silico* Predicted BBB permeability[c]	CNS Category[d]	Literature CNS category[b]
SIEH10	4.796 ± 0.075	NA	0.181	CNS+	NA
Donepezil	7.504 ± 0.305	6.80	0.188	CNS+	CNS+
Selegiline	6.417 ± 0.205	5.69	4.435	CNS+	CNS+
Imipramine[e]	14.922 ± 0.131	13	2.920	CNS+	CNS+
Tenoxicam[e]	1.267 ± 0.168	0.1	0.095	CNS-	CNS-

[a] P_e values as mean ± SD of two independent experiments in duplicate.
[b] Values are cited from Di *et.al.*, 2003.
[c] BBB permeability using PreADMET web-based server (accessed on 08.08.2024).
[d] CNS+ ($P_e > 4.0 \times 10^{-6}$ cm/s), CNS± ($P_e > 2.0 \times 10^{-6}$ cm/s < 4.0×10^{-6} cm/s), CNS- ($P_e < 2.0 \times 10^{-6}$ cm/s)[b]
[e] Used as positive and negative permeability controls respectively.

4.4.2.1.7. Cell-based neurotoxicity assay

The compound **SIEH10** was evaluated for its cytotoxicity against non-cancerous fibroblast (L929) cells and neurotoxicity against neuroblastoma cell lines (SH-SY5Y). The cells were treated for 24 h with different concentrations (0.1, 1, 10, 50 and 100 μM) of compound **SIEH10** and MTT assay was performed post treatment. The obtained results indicate that compound **SIEH10** was non-toxic to the fibroblast and neuroblastoma cells up to 10 μM concentration. The percent cell viability graph versus the concentration of the compound was constructed and indicated in **Figures 4.8A & 4.8B**. These observations suggest that the compound **SIEH10** is toxic to neuroblastoma cells at the given concentration.

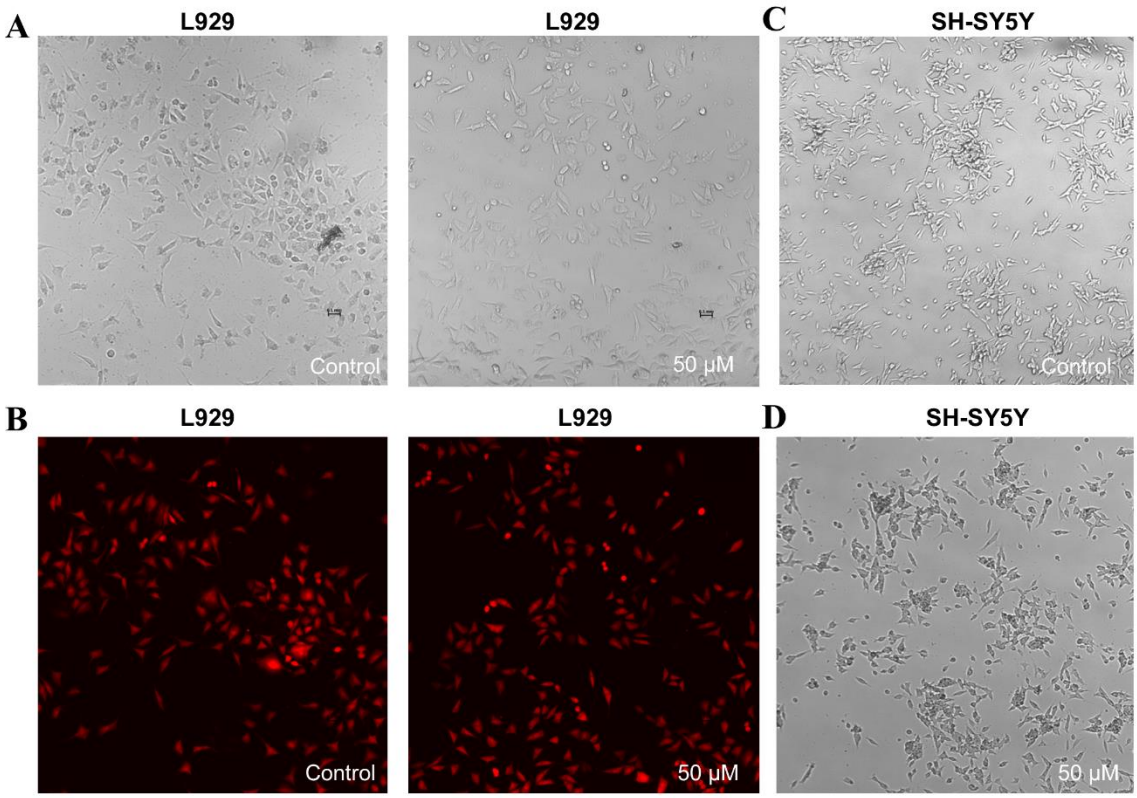

Figure 4.7. *In vitro* neurotoxicity assay of compound **SIEH10** in fibroblast (L929) and neuroblastoma (SH-SY5Y) cells; A) inverted microscopic brightfield image of L929 cell 24 h post-treatment with compound **SIEH10** at 0 µM (Control) and 50 µM concentration; B) inverted microscopic fluorescence image of L929 cell 24 h post-treatment with compound **SIEH10** at 0 µM (Control) and 50 µM concentration; C) microscopic brightfield image of SH-SY5Y cell 24 h post-treatment with compound **SIEH10** at 0 µM (Control) and D) 50 µM concentration.

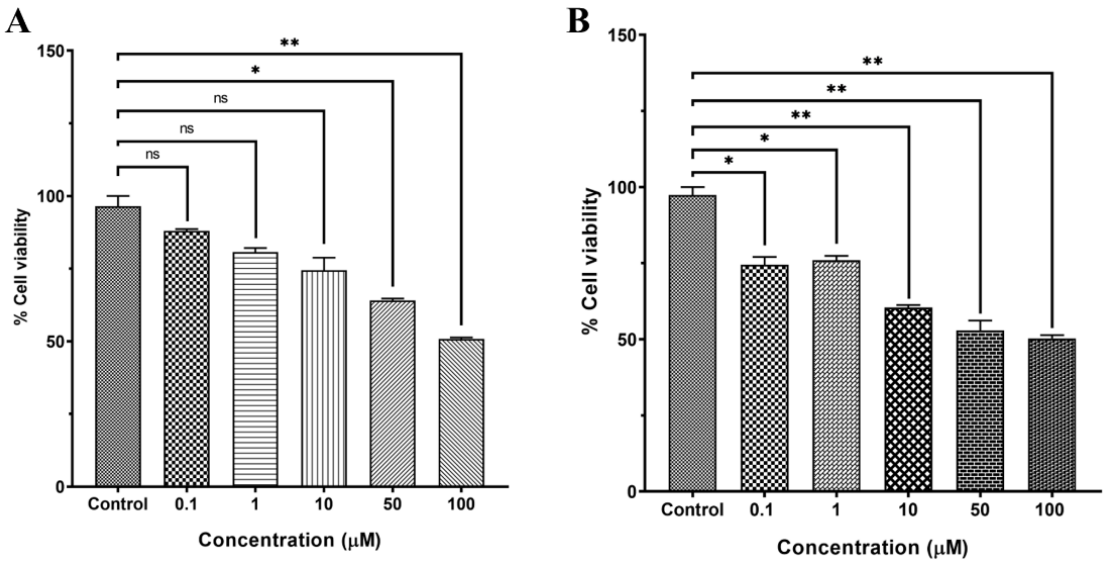

Figure 4.8. Cell viability graphs of compound **SIEH10** against A) Fibroblast (L929); and B) Neuroblastoma cell line (SH-SY5Y).

4.4.2.1.8. Neuroprotection assay using neuroblastoma cell line

The neuroprotective potential of compound **SIEH10** was evaluated against dexamethasone-induced oxidative stress and apoptosis in neuroblastoma cell lines (SH-SY5Y). Neuroblastoma cells were treated with 2 μM dexamethasone solution before treatment with different concentrations (0.25, 100 and 200 nM) of test compound **SIEH10** for 72 h. Subsequently, an MTT assay was performed to assess cell viability due to action of dexamethasone and neuroprotection due to the compound. The cell viability graph in **Figure 4.9** indicates that significant recovery was observed with different doses of the compound **SIEH10**.

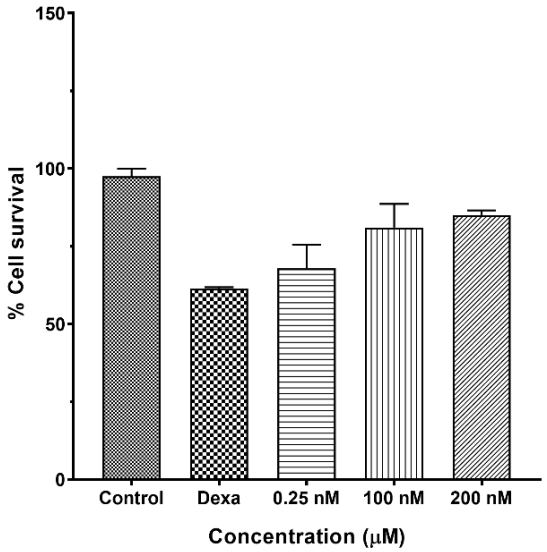

Figure 4.9. *In vitro* neuroprotection assay of compound **SIEH10** in SH-SY5Y cells against dexamethasone-induced oxidative stress, % cell survival vs. different concentrations (0.25, 100 and 200 nM) of compound **SIEH10** with 2 μM concentration of dexamethasone.

4.4.2.2. *In vivo* studies

4.4.2.2.1. Scopolamine-induced amnesia model (Y-maze test)

The *in vivo* neuroprotective efficacy of the compound **SIEH10** was evaluated at a dose of 5 mg/kg using a scopolamine-induced amnesia model while the change in the animal behavior and memory impairment was evaluated using the Y-maze test. The percentage of alternation was significantly decreased ($p < 0.05$) in the scopolamine (SCO)-treated group

compared to the control group, indicating the cognitive impairment induced by scopolamine. Unfortunately, no significant improvement in % spontaneous alternation was observed in the groups treated with **SIEH10** suggesting a poor or minute reversal of scopolamine-induced memory deficit. **Figure 4.10** indicates that compound **SIEH10** possesses weak or no *in vivo* neuroprotective activity against the scopolamine-induced amnesia model.

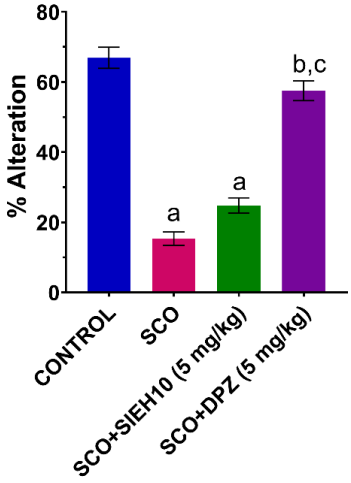

Figure 4.10. Effect of compound **SIEH10** on scopolamine-induced cognition and memory impairment showing effect on spontaneous alteration A) % $^{a}P < 0.05$ vs. control; $^{b}P < 0.05$ vs. scopolamine; $^{c}P < 0.05$ vs. compound **SIEH10** (5 mg/kg), $^{d}P < 0.05$ vs. DPZ (5 mg/kg).

4.4.3. Computational studies

4.4.3.1. Molecular docking

The molecular docking studies of all the test molecules and co-crystallized ligands have been carried out to understand the 3D orientation of 2D molecular interaction of ligands with active site residues. The molecular docking of each co-crystallized ligand was performed to validate the docking protocol and system suitability. Protein crystal structures of MAO-A (PDB ID: 2Z5X), MAO-B (PDB ID: 2V5Z), AChE (PDB ID: 4EY7), and BChE (7PDB ID: AWG) having good resolution were obtained from Protein Data Bank and utilized for molecular studies [19, 155, 156, 189]. Molecular interaction results were

obtained as binding energy (ΔG) and calculated inhibition constant (K_i) are provided in **Table 4.5**.

Table 4.5. Molecular docking results of compounds **SEH01-SEH11** and **SIEH01-SIEH11** against MAO-A, MAO-B, AChE and BChE

Compd. code	MAO-A (2Z5X)		MAO-B (2V5Z)		AChE (4EY7)		BChE (7AWG)	
	ΔG (kcal/mol)	Ki (μM)	ΔG (kcal/mol)	Ki (μM)	ΔG (kcal/mol)	Ki (μM)	ΔG (kcal/mol)	Ki (μM)
SEH01	-9.5	0.108	-10.00	0.047	-8.29	0.839	-9.17	0.189
SEH02	-9.33	0.145	-9.85	0.061	-7.68	2.330	-8.09	1.170
SEH03	-9.59	0.094	-9.69	0.078	-8.55	0.543	-7.84	1.800
SEH04	-10.18	0.035	-10.32	0.027	-8.52	0.566	-8.77	0.373
SEH05	-9.53	0.103	-8.85	0.324	-8.42	0.676	-7.24	4.950
SEH06	-9.19	0.184	-9.29	0.155	-8.24	0.913	-9.24	0.168
SEH07	-9.38	0.133	-9.80	0.065	-8.48	0.611	-7.89	1.640
SEH08	-9.05	0.234	-9.83	0.063	-7.97	1.430	-7.61	2.630
SEH09	-8.00	1.380	-9.81	0.064	-8.64	0.464	-7.95	1.480
SEH10	-9.25	0.166	-9.70	0.077	-7.75	2.100	-8.57	0.521
SEH11	-9.50	0.109	-8.49	0.597	-8.82	0.345	-7.74	2.130
SIEH01	-10.00	0.047	-9.50	0.108	-8.06	1.230	-8.18	1.010
SIEH02	-9.41	0.126	-9.24	0.168	-8.42	0.670	-8.12	1.110
SIEH03	-9.24	0.168	-10.00	0.046	-8.65	0.458	-7.84	1.790
SIEH04	-9.69	0.080	-10.07	0.042	-9.11	0.210	-8.28	0.857
SIEH05	-7.98	1.400	-9.57	0.096	-9.17	0.191	-8.16	1.040
SIEH06	-9.25	0.166	-9.40	0.129	-9.03	0.240	-7.98	1.420
SIEH07	-9.06	0.229	-9.63	0.087	-8.49	0.595	-8.40	0.692
SIEH08	-9.18	0.187	-9.40	0.129	-8.50	0.589	-8.14	1.090
SIEH09	-9.14	0.199	-9.59	0.093	-8.90	0.300	-7.92	1.570
SIEH10	-9.72	0.075	-9.99	0.047	-9.30	0.153	-7.82	1.850
SIEH11	-8.57	0.521	-10.12	0.038	-8.77	0.373	-7.11	6.120
Std.[a]	-7.70	2.280	-8.95	0.277	-10.49	0.020	-9.07	0.225

[a] Molecular Docking score of co-crystallized ligand (MAO-A, PDB ID: 2Z5X, Harmine; MAO-B, PDB ID: 2V5Z, Safinamide; AChE, PDB ID: 4EY7, Donepezil; BChE, PDB ID: 7AWG, S6Q).

4.4.3.1.1. Molecular docking studies with MAO-A

The molecular docking results of compounds **SEH01-SEH11** and **SIEH01-SIEH11** against MAO-A revealed the way of orientation and interaction of these molecules within the active site. 3D superimposition image of all compounds confirmed that all molecules were well accommodated in the MAO-A active site and occupied the same cavity as the co-crystallized standard inhibitor (harmine). The eugenol and isoeugenol moiety of most

of the ligands was oriented toward the entrance cavity of the active site while the variable aryl moiety was pointed towards the isoalloxazine ring of the FAD (co-factor; **Figure 4.11A**).

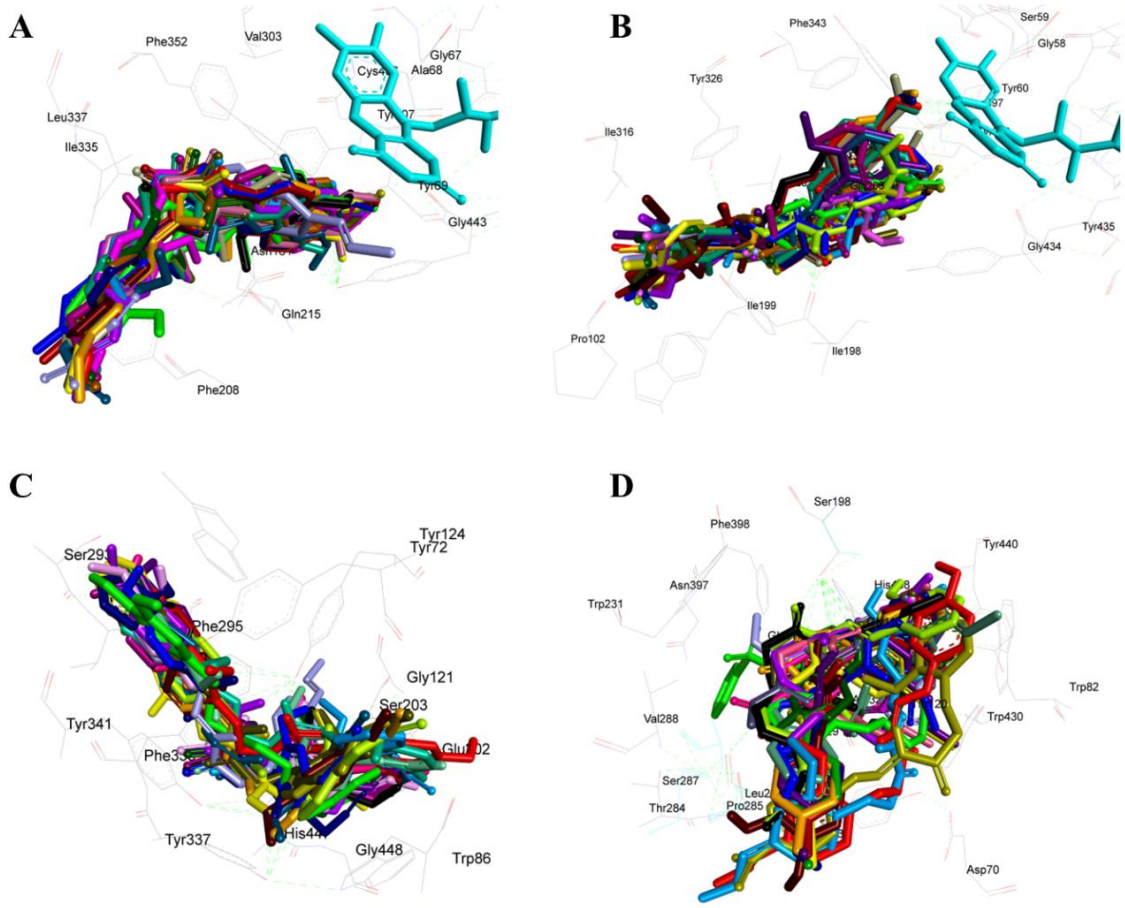

Figure 4.11. 3D orientation map of ligands **SEH01-SEH11** and **SIEH01-SIEH11** in the active site of respective targets; A) 3D super imposition of compounds **SEH01-SEH11** and **SIEH01-SIEH11** in the active site of MAO-A; B) 3D accommodation of compounds **SEH01-SEH11** and **SIEH01-SIEH11** in MAO-B active site; C) 3D array of ligands **SEH01-SEH11** and **SIEH01-SIEH11** within the active gorge of AChE; D) Ligand orientation or 3D superimposition image of compounds **SEH01-SEH11** and **SIEH01-SIEH11** in active site of BChE.

4.4.3.1.2. Observed interactions of compound SIEH10 with MAO-A

The visualization of 3D superimposition image of docked compound **SIEH10** within the active site of MAO-A indicates that compound **SIEH10** was well accommodated within the active site. The isoeugenol moiety of the compound was orientated towards the entrance

of the cavity whereas the aryl moiety of the molecule was pointed towards the isoalloxazine ring of FAD (**Figure 4.12A**). 2D interaction map show types of interactions that stabilize ligands within active site. These interactions involve pi-alkyl, pi-pi stacking, pi-pi T shaped and van der Waals interaction. The methoxy group of vanillin moiety in the ligand interacts with Tyr407, Tyr444, FAD and Gly 443 through pi-sigma and carbon-hydrogen bonding interaction, respectively. Tyr407 also interacts with the terminal aryl ring through pi-pi T-shaped interaction. The methoxy group of isoeugenol moiety interacts with Ile180 through pi-alkyl interaction while the aromatic ring interacts with Phe208, Cys323, Leu337 and Ile335 through pi-pi stacking, pi-alkyl and pi-sigma interactions, respectively. The propenyl moiety of ligand interacts with Leu97, Ala111 and Val210 through pi-alkyl interaction while residues Tyr69, Gly110, Asn181, Tyr197, Ile207, Ser209, Gln215, Thr336, Met350 and Phe352 interacts through van der Waals interactions (**Figure 4.12C**).

4.4.3.1.3. Molecular docking studies with MAO-B

3D superimposition image of compounds **SEH01-SEH11** and **SIEH01-SIEH11** against MAO-B indicates that all the ligands were well lodged within the active site and lie in the same cavity as the reference inhibitor (safinamide). The eugenol and isoeugenol moiety of most of the compounds were oriented towards the entrance cavity of the active site whereas the variable aryl ring isoalloxazine ring of FAD was pointed towards (substrate cavity, **Figure 4.11B**).

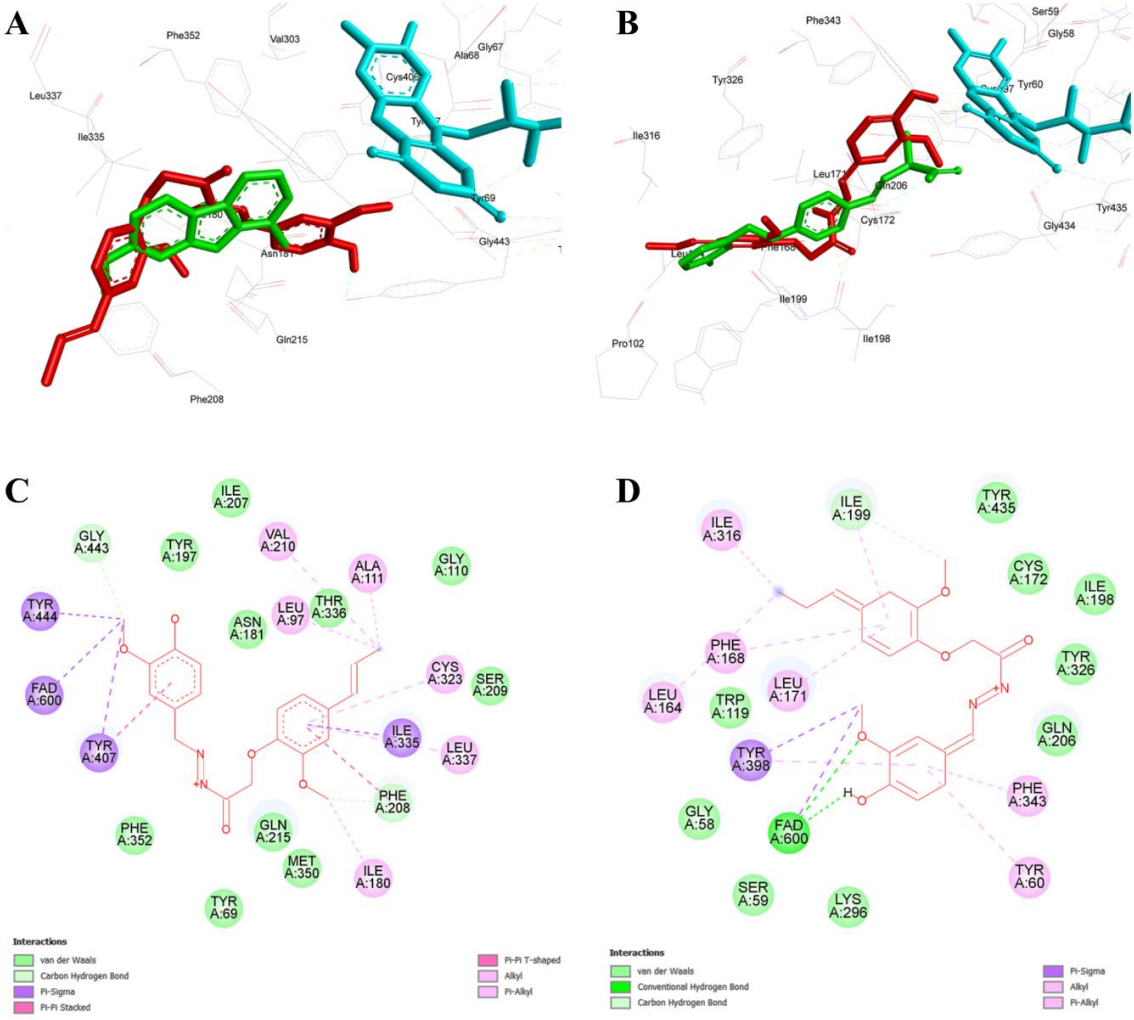

Figure 4.12. 3D alignment and 2D interaction map of compound **SIEH10** in the active site gorge of MAO-A and MAO-B; A) 3D alignment of compound **SIEH10** (red) and harmine (green) in the active site gorge of MAO-A; B) 2D interaction map of compound **SIEH10** with residues of MAO-A active site; C) 3D alignment of compound **SIEH10** (red) and safinamide (green) in the active site gorge of MAO-B; D) 2D interaction map of compound **SIEH10** with residues of MAO-B active site.

4.4.3.1.4. Observed interactions of compound SIEH10 with MAO-B

The analysis of the 3D orientation image of compound **SIEH10** resulted in the molecule was wisely accommodated within the active site gorge of MAO-B and occupied the same cavity as the reference inhibitor safinamide. The isoeugenol moiety of compound **SIEH10** was pointed towards the entrance of the active site while variable aryl moiety was oriented towards the isoalloxazine ring of FAD (**Figure 4.12B**). Further, the 2D interaction map of compound **SIEH10** shows hydrogen bonding and hydrophobic interactions with active site

residues. The methoxy group on the terminal aryl ring of the ligand interacts with FAD and Tyr398 through pi-sigma and hydrogen bonding interactions. FAD also interacts with a hydroxyl group of ligands through hydrogen bonding while the terminal aryl ring interacts with Tyr60, Phe343 and Tyr398 through pi-alkyl interaction. Ile199 interacts with the phenyl ring of isoeugenol moiety and methoxy group through pi-alkyl and carbon-hydrogen bonding interactions, respectively. The phenyl ring of isoeugenol moiety also interacts with Phe168 and Leu171 through pi-alkyl interaction while the propenyl group interacts with Leu163 and Ile316 through pi-alkyl interaction. Additionally, residues Gly58, Ser59, Trp119, Cys172, Ile198, Gln206, Phe343, Tyr398 and Tyr435 interacts through van der Waals interactions (**Figure 4.12D**).

4.4.3.1.5. Molecular docking studies with AChE

The molecular docking studies of compounds **SEH01-SEH11** and **SIEH01-SIEH11** within the active site of AChE revealed the binding pattern and orientation of ligands. All the docked ligands were well facilitated within the active site and lodged in the same cavity as the co-crystallized ligand (donepezil). The variable aryl moiety of most of the ligands was oriented towards the bottom gorge of the active site while of eugenol and isoeugenol moiety was pointed towards the opening of the active site (**Figure 4.11C**).

4.4.3.1.6. Observed interactions of compound SIEH10 with AChE

The examination of the 3D orientation image of compound **SIEH10** revealed proper accommodation of the compound within the active site gorge of the enzyme AChE and occupied the same position as reference inhibitor donepezil. The isoeugenol moiety was oriented toward the entrance of the active site while the variable aryl ring was pointed toward the bottom gorge of the site (**Figure 4.13A**). Apart from orientation compound **SIEH10** was stabilized within the active site by hydrophobic interactions including hydrogen bonding, pi-alkyl, pi-pi stacking and van der Waals interactions. The methoxy

group at the terminal aryl ring and aryl ring of the ligand interacts with Trp86 through pi-alkyl and pi-pi stacking interaction, respectively. The methoxy group at isoeugenol moiety interacts with Tyr72, Trp286 and Tyr341 through pi-alkyl interaction while Tyr124 interacts through hydrogen bonding interaction. The aromatic ring of isoeugenol interacts with Tyr341 through pi-pi stacking interaction while propenyl interacts with Trp286 through pi-alkyl interaction. Further, residues Gly121, Glu202, Ser203, Ser293, Val294, Phe295, Tyr337, Phe338 and His447 interacts through van der Waals forces (**Figure 4.13C**).

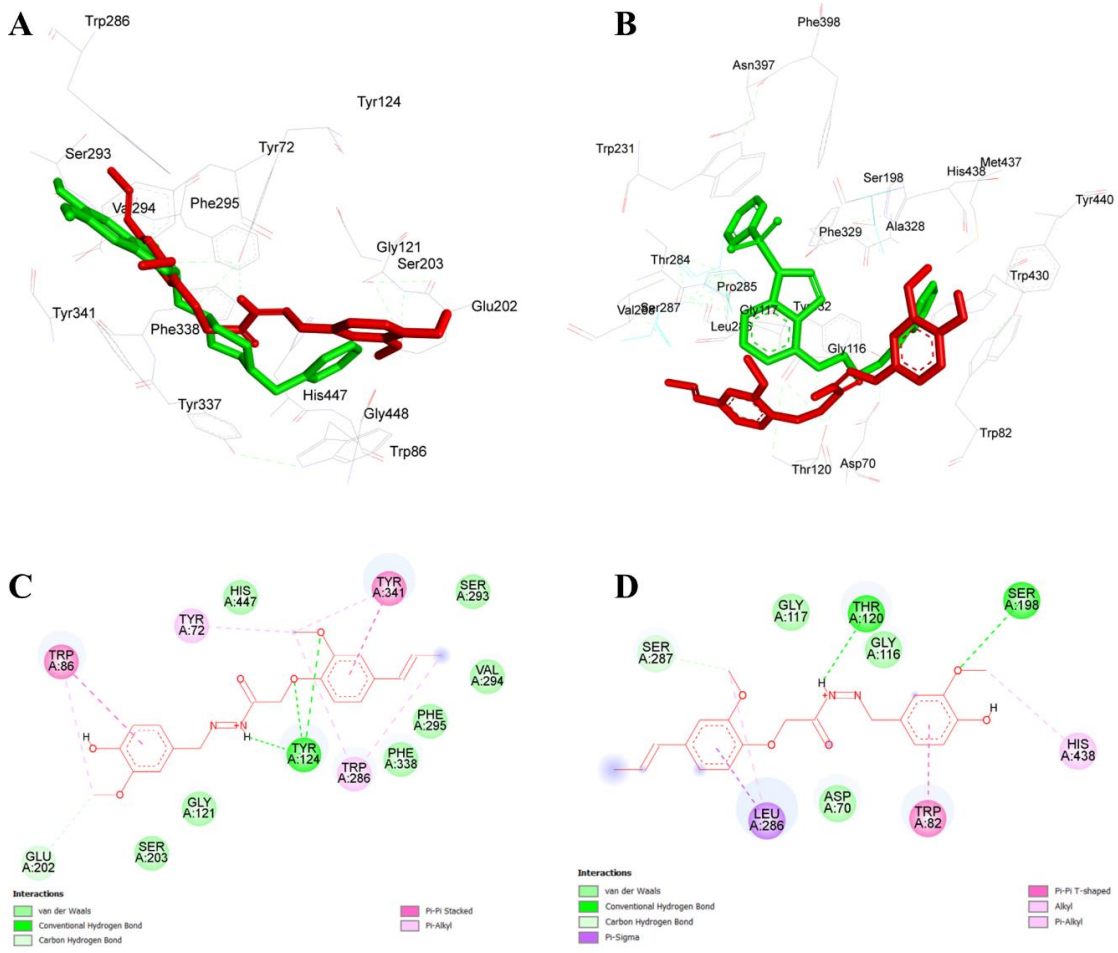

Figure 4.13. 3D alignment and 2D interaction map of compound **SIEH10** in the active site gorge of AChE and BChE; A) 3D alignment of compound **SIEH10** (red) and donepezil (green) in the active site gorge of AChE; B) 2D interaction map of compound **SIEH10** with residues of AChE active site; C) 3D alignment of compound **SIEH10** (red) and S6Q (green) in the active site gorge of BChE; D) 2D interaction map of compound **SIEH10** with residues of BChE active site.

4.4.3.1.7. Molecular docking studies with BChE

The visual inspection of docked 3D superimposition image of compounds **SEH01-SEH11** and **SIEH01-SIEH11** indicate that all the ligands were appropriately accommodated within the active site of the target BChE. The variable aryl moiety of most of the ligands was pointed towards the bottom gorge of the site while eugenol and isoeugenol moiety was oriented towards the surface of the protein or opening of the active site (**Figure 4.11D**).

4.4.3.1.8. Observed interactions of compound SIEH10 with BChE

The visual inspection of the 3D alignment image of compound **SIEH10** indicates that compound **SIEH10** was well housed within the active site gorge of BChE and occupied the same position as reference inhibitor S6Q (**Figure 4.13C**). The 2D interaction map of compound **SIEH10** shows that the molecule was accommodated and stabilized by hydrogen bonding and hydrophobic interactions. The methoxy group of vanillin moiety formed a hydrogen bond with Ser198 while with His438 it formed a pi-alkyl interaction. Terminal aryl ring interacts with Trp82 through pi-pi T-shaped interaction while imine nitrogen formed a hydrogen bond with Thr120. The methoxy group of isoeugenol moiety interacts with Ser287 through carbon-hydrogen bonding while alkyl interaction was observed with Leu286. The benzene ring of isoeugenol moiety formed pi-sigma interaction was observed with Leu286. Furthermore, van der Waals interactions were observed with residues Asp70, Gly116, and Gly117 (**Figure 4.13D**).

4.4.3.2. Molecular dynamics simulation

The protein-ligand binding strength and reliability of docking results were validated by conducting molecular dynamic simulation studies for compound **SIEH10-**MAO-B (PDB ID:2V5Z) complex and compound **SIEH10**-AChE (PDB ID: 4EY7) complex. The Desmond module (Version 12.7.156, Schrodinger Release 2021.1: Desmond Molecular Dynamics System, D. E. Shaw Research, New York, NY, 2021) was employed for running

100 ns of MD simulation. The preparation of all the input files, processing of simulation results and visual analysis of results were done through the Maestro graphical user interface (Maestro, Schrodinger, LLC, New York, NY, 2021).

Post simulation, protein-ligand complexes were analyzed for root mean square deviation (RMSD), root mean square fluctuation (RMSF), ligand-protein contacts, protein-ligand contact histogram, and protein-ligand contact timeline along with to understand if any type of significant conformational changes occurred in the protein structure during simulation.

4.4.3.2.1. MD simulation of compound SIEH10-MAO-B complex

The visual inspection of simulated MAO-B-compound **SIEH10** complex revealed that compound **SIEH10** interacts with Cys172 through hydrophobic interaction for 36 % of total simulation while Phe343, Tyr398 and Tyr435 interact through pi-pi stacking for 18 %, 60 % and 45 % of the simulation period, respectively (**Figure 4.14A**). Compound **SIEH10** was well stabilized by hydrogen bonding interactions with Cys172, Ile198, Gln206, Tyr326, and Gly434; hydrophobic interactions with Leu88, Phe99, Phe103, Pro104, Pro105, Trp119, Leu164, Leu167, Phe168, Leu171, Ile198, Ile199, Ile316, Tyr326, Phe343, Tyr398 and Tyr435; and water bridges with Gly57, Ser59, Leu171, Ile198, Gln206, Lys296, Tyr326, Tyr398 and Tyr435 (**Figure 4.14C**). A good degree of contact was observed with crucial residues of the active site including Leu171, Cys172, Ile199, Gln206, Tyr326, Tyr398, Gly434 and Tyr435 (**Figure 4.14B**). The RMSD graph of protein and ligand shows that the simulation system stabilized near 20 ns and remained stable for the rest of the period (**Figure 4.14D**).

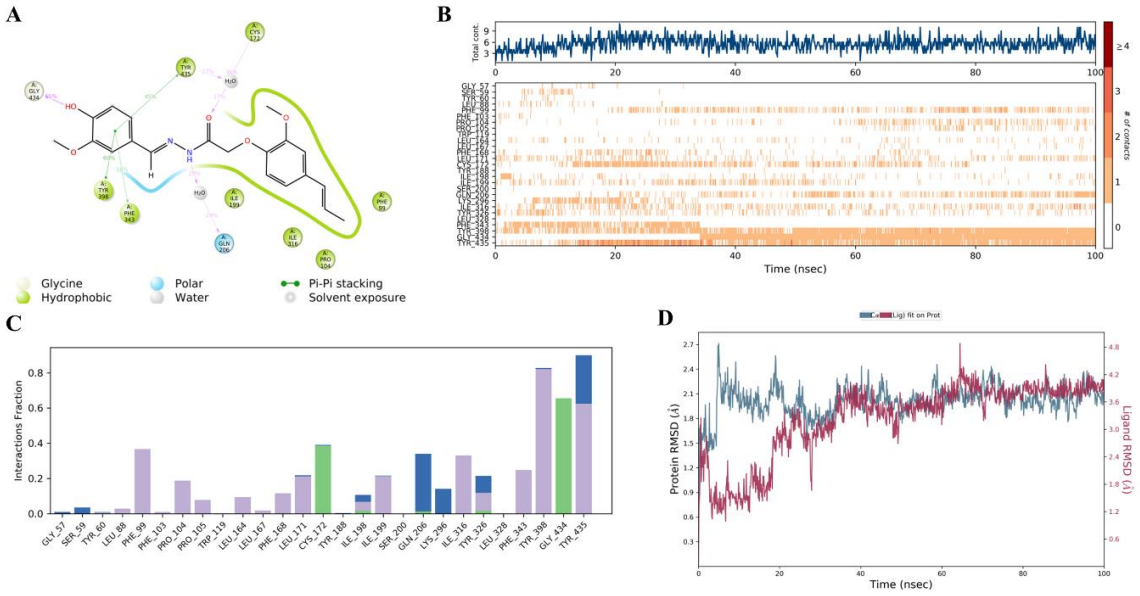

Figure 4.14. Protein-ligand contacts map of compound **SIEH10** generated during MD simulation with MAO-B (PDB ID: 2V5Z); A) 2D protein-ligand contact diagram of compound **SIEH10-**MAO-B complex; B) Protein-ligand interaction and contact timeline; C) Protein-ligand contact histogram (hydrogen bonding: green bars, hydrophobic interaction: violet bars and water bridges: blue bars) with surrounding residues of MAO-B active site; D) Protein (blue) and ligand (maroon) RMSD graph.

4.4.3.2.2. MD simulation of compound SIEH10-AChE complex

The visual examination of simulated AChE-compound **SIEH10**-complex disclosed that compound **SIEH10** interacts with Phe295 through hydrophobic interaction for 99 % of the time while with Trp286 and Tyr337 through pi-pi stacking for 91 %, and 57 % of the total simulation period, respectively (**Figure 4.15A**). Compound **SIEH10** was well stabilized by hydrogen bonding interactions with Gly121, Gly122, Ser203, Phe295, Arg296 and Tyr341; hydrophobic interactions with Tyr72, Leu76, Trp86, Tyr124, Trp286, Phe295, Phe297, Tyr337, Phe338 and Tyr341; and water bridges with Asp74, Gly121, Gly122, Ser125, Glu202, Ser203, Arg296, Tyr337, Tyr341 and His447 (**Figure 4.15B**). A decent degree of contact was observed with crucial residues of active site including Trp86, Tyr124, Trp286, Phe295, Tyr337 and Tyr341 (**Figure 4.15C**). The RMSD graph of protein and ligand shows that the simulation system was fully stable throughout the simulation period (**Figure 4.15D**).

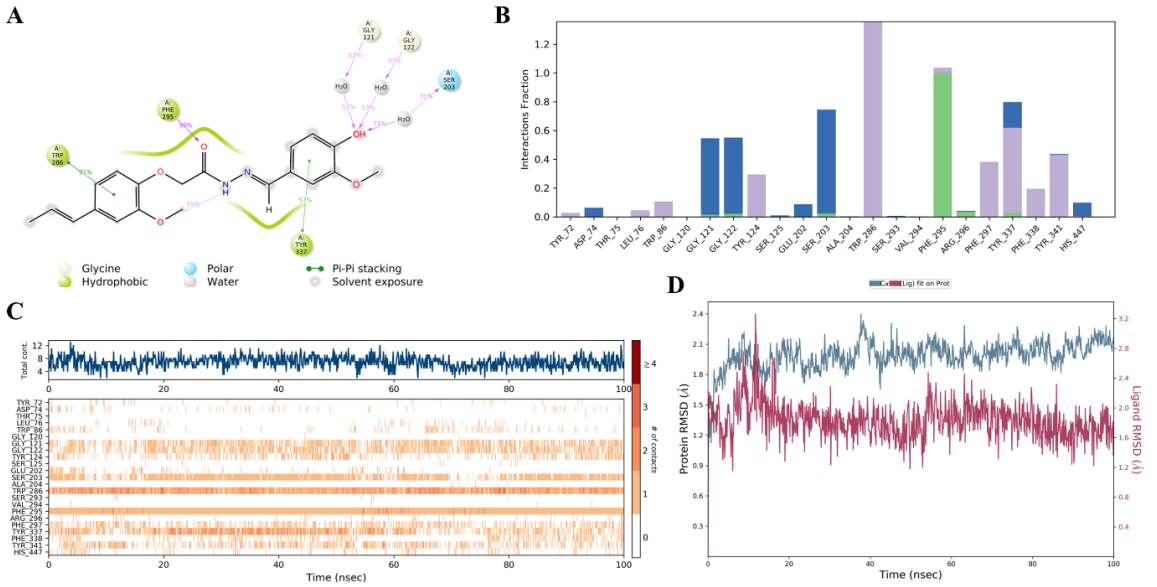

Figure 4.15. Protein-ligand contacts map of compound **SIEH10** generated during MD simulation with AChE (PDB ID: 4EY7); A) 2D protein-ligand contact diagram of compound **SIEH10** -AChE complex; B) Protein-ligand contact histogram (hydrogen bonding: green bars, hydrophobic interaction: violet bars and water bridges: blue bars) with surrounding residues of AChE active site; C) Protein-ligand interaction and contact timeline; D) Protein (blue) and ligand (maroon) RMSD graph.

4.4.3.3. Ligand binding efficiency

Ligand binding efficiency is the ratio of free energy of binding over the total number of heavy atoms in a ligand. The size and the number of heavy atoms in a ligand have an impact on the potency of the molecule and are regarded as an imperative metric in drug discovery. A compromise in the potency of ligands is observed as the number of heavy atoms increased after a certain extent. Ligands with the very high number of heavy atoms or very few atoms are not suitable ligands for efficient binding. The calculated ligand binding efficiency of compounds **SEH01-SEH11** & **SIEH01-SIEH11** against MAO-A, MAO-B and AChE lies near 0.35 along with reference inhibitor compounds which indicates that these compounds fall under suitable binder and are in acceptable range (**Figure 4.16**) [29].

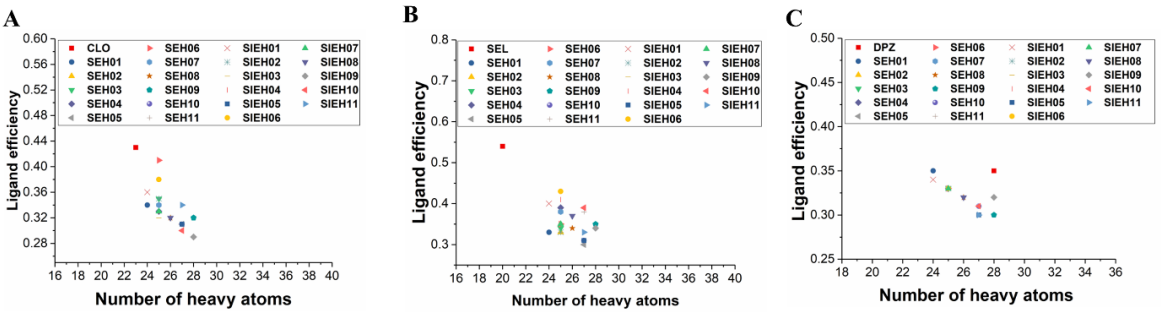

Figure 4.16. Ligand binding efficiency of compounds **SEH01-SEH11 & SIEH01-SIEH11** against A) MAO-A; B) MAO-B and C) AChE.

4.4.3.4. Predicted ADMET properties

ADMET properties of the synthesized compounds (**SEH01-SEH11** and **SIEH01-SIEH11**) were predicted to understand the pharmacokinetic profile of the molecules. These predicted properties provide us an insight into how these new molecules are going to behave in the living system and predicted ADME parameters are given in **Table 4.6**. Predicted human intestinal absorption (HIA) falls between 93 to 96 % which indicates that compounds will be well absorbed from the GI tract. All the compounds show moderate to strong plasma protein binding (PPB) and lie in the range of 88 to 97 %. Negative values of skin permeability indicate that compounds are not suitable for transdermal delivery. Most of the compounds displayed moderate Caco2 cell permeability which means compounds will pass through the intestinal epithelial barrier. Most of the molecules show moderate MDCK cell and blood-brain barrier (BBB) permeability. All the compounds were predicted as inhibitors of liver enzymes CYP2C9, CYP2C19 and CYP3A4 except compounds **SEH05** and **SIEH05**.

Table 4.6. Predicted ADME properties of compounds **SEH01-SEH11** and **SIEH01-SIEH11**

Compd. code	HIA (%)	Caco2	MDCK (nm/s)	SP (logKp, cm/h)	BBB	PPB (%)	CYP2C9	CYP2C19	CYP3A4
SEH01	95.70	26.46	81.081	-2.21	0.239	95.32	inhibitor	inhibitor	inhibitor
SEH02	95.70	32.82	125.131	-2.48	0.346	90.87	inhibitor	inhibitor	inhibitor
SEH03	96.10	40.94	61.868	-2.26	0.529	89.62	inhibitor	inhibitor	inhibitor
SEH04	96.42	40.40	0.448	-2.15	0.578	93.14	inhibitor	inhibitor	inhibitor
SEH05	95.27	5.99	141.922	-2.20	0.102	92.34	non	non	non
SEH06	93.64	22.49	101.329	-2.43	0.458	88.64	inhibitor	inhibitor	inhibitor
SEH07	93.64	4.88	139.142	-2.45	0.525	90.26	inhibitor	inhibitor	inhibitor
SEH08	95.96	26.11	122.052	-5.39	0.178	92.99	inhibitor	inhibitor	inhibitor
SEH09	96.39	51.83	60.535	-2.46	0.108	88.97	inhibitor	inhibitor	inhibitor
SEH10	93.96	19.23	126.213	-2.51	0.247	89.06	inhibitor	inhibitor	Inhibitor
SEH11	93.96	16.72	126.213	-2.51	0.250	89.38	inhibitor	inhibitor	inhibitor
SIEH01	95.70	26.46	80.587	-2.31	0.166	97.47	inhibitor	inhibitor	inhibitor
SIEH02	95.70	32.82	127.614	-2.59	0.239	92.1	inhibitor	inhibitor	inhibitor
SIEH03	96.10	40.94	60.629	-2.36	0.415	89.99	inhibitor	inhibitor	inhibitor
SIEH04	96.42	40.40	0.469	-2.24	0.463	92.41	inhibitor	inhibitor	inhibitor
SIEH05	95.27	5.99	144.315	-2.29	0.071	93.22	non	non	non
SIEH06	93.64	22.49	102.802	-2.51	0.361	90.09	inhibitor	inhibitor	inhibitor
SIEH07	93.64	4.88	141.208	-2.53	0.395	91.8	inhibitor	inhibitor	inhibitor
SIEH08	95.96	26.11	123.696	-2.45	0.107	94.2	inhibitor	inhibitor	inhibitor
SIEH09	96.39	51.83	60.234	-2.58	0.065	89.54	inhibitor	inhibitor	inhibitor
SIEH10	93.96	19.23	127.486	-2.61	0.181	90.1	inhibitor	inhibitor	inhibitor
SIEH11	93.96	16.72	127.486	-2.61	0.184	90.47	inhibitor	inhibitor	inhibitor
E20	97.95	55.51	0.138	-3.04	0.187	84.61	non	non	non
SAG	93.59	10.27	16.903	-3.11	0.134	89.45	non	non	inhibitor

HIA = Human intestinal absorption (%), Rule: 0-20 (poor), 20-70 (moderate) and 70-100 (well); **Caco2** = *In vitro* permeability of Caco2 cell (nm/s), Rule: <4 (low), 4-70 (moderate), >70 (high); **MDCK** = Maden Darby canine kidney cell permeability (nm/s), Rule: <25 (low), 25-500 (moderate), >500 (high); **SP**: *In vitro* skin permeability (cm/h); **BBB** = Blood brain barrier permeability (Cbrain/Cblood), Rule: <0.1 (low), 0.1-2.0 (moderate), >2.0 (High); **PPB** = *In vitro* plasma protein binding (%), Rule: <90 (moderate bound), >90 (Strong bound); **E20** = Donepezil; **SAG** = Safinamide; non = non-inhibitor.

Furthermore, all the compounds were subjected to *in silico* toxicity prediction using the PreADMET web server and the obtained results are mentioned in **Table 4.7**. Predicted mutagenicity using the Ames test model showed all the compounds as mutagen whereas the mouse carcinogenicity predicted all compounds as non-carcinogenic. Most compounds were predicted as non-carcinogenic for rat carcinogenicity except compounds **SEH04** (predicted as carcinogenic). Additionally, the predicted hERG inhibition show compounds

SEH01, **SEH05**, **SEH06** and **SIEH01** having a low risk for hERG inhibition whereas compounds **SEH10**, **SEH11**, **SIEH10**, and **SIEH11** have a high risk for hERG inhibition and the rest of the compounds displayed medium risk for hERG inhibition [176].

Table 4.7. Predicted toxicity properties of compounds **SEH01-SEH11** and **SIEH01-SIEH11**

Compd. Code	Ames test	Carcinogenicity (Mouse)	Carcinogenicity (Rat)	hERG inhibition
SEH01	Mutagen	Negative	Negative	low risk
SEH02	Mutagen	Negative	Negative	medium risk
SEH03	Mutagen	Negative	Negative	medium risk
SEH04	Mutagen	Negative	Positive	medium risk
SEH05	Mutagen	Negative	Negative	low risk
SEH06	Mutagen	Negative	Negative	low risk
SEH07	Mutagen	Negative	Negative	medium risk
SEH08	Mutagen	Negative	Negative	medium risk
SEH09	Mutagen	Negative	Negative	medium risk
SEH10	Mutagen	Negative	Negative	high risk
SEH11	Mutagen	Negative	Negative	high risk
SIEH01	Mutagen	Negative	Negative	low risk
SIEH02	Mutagen	Negative	Negative	medium risk
SIEH03	Mutagen	Negative	Negative	medium risk
SIEH04	Mutagen	Negative	Positive	medium risk
SIEH05	Mutagen	Negative	Negative	medium risk
SIEH06	Mutagen	Negative	Negative	medium risk
SIEH07	Mutagen	Negative	Negative	medium risk
SIEH08	Mutagen	Negative	Negative	medium risk
SIEH09	Mutagen	Negative	Negative	medium risk
SIEH10	Mutagen	Negative	Negative	high risk
SIEH11	Mutagen	Negative	Negative	high risk
E20	Mutagen	Negative	Negative	medium risk
SAG	Mutagen	Positive	Negative	medium risk

Ames test: Ames test for mutagenicity in Salmonella typhimurium, **Carcinogenicity (Mouse):** 2 years carcinogenicity bioassay in mouse, **Carcinogenicity (Rat):** 2 years carcinogenicity bioassay in rat, **hERG Inhibition:** *In Vitro* Human Ether-a-go-go Related Gene Channel Inhibition; **E20 =** Donepezil, **SAG** = Safinamide.

4.5. Summary

In summary, a library of 22 eugenol and isoeugenol-derived carbohydrazones (compounds **SEH01-SEH11** & **SIEH01-SIEH11**) was designed by molecular hybridization of our in-house lead compound (**SMH06**) and eugenol to improve MAO-B and AChE inhibitory potential of resultant analogs. The structure of in-house lead was modified by replacing of

benzodioxole/sesamol moiety with eugenol moiety having a methoxy and an allyl group that can offer inhibitory activity against MAO-B and AChE.

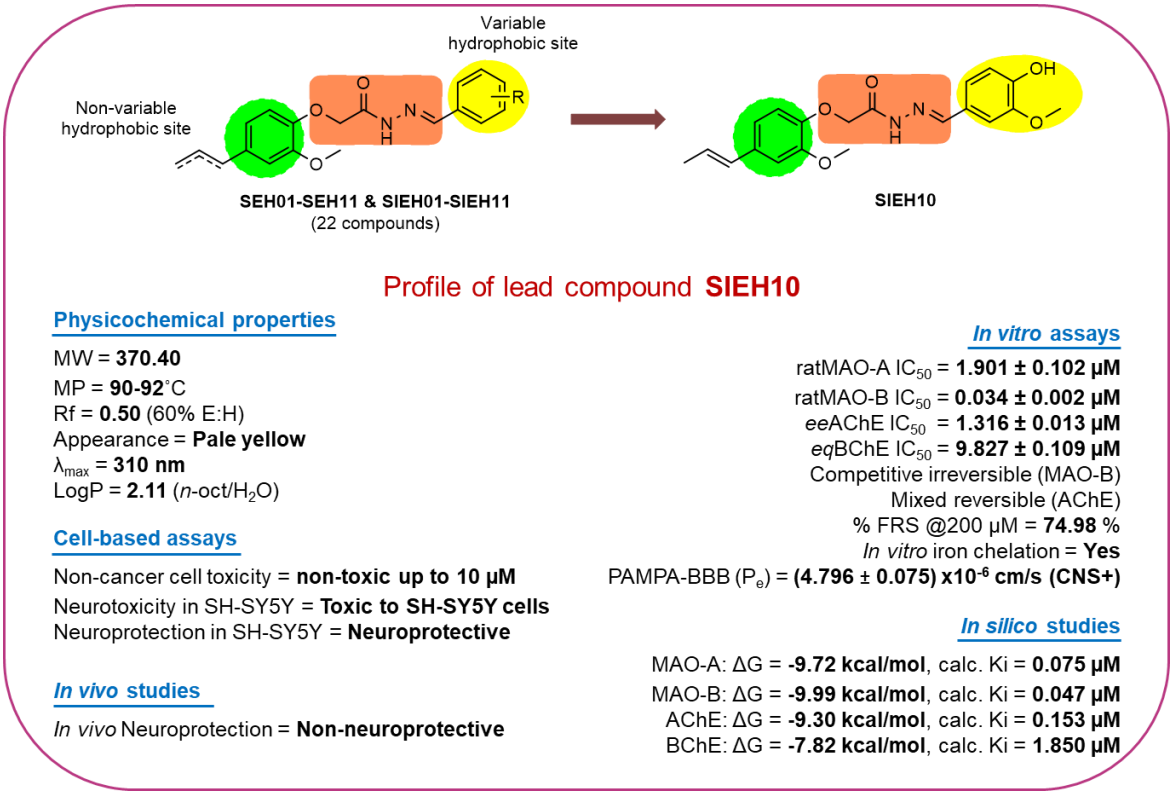

Figure 4.17. Summary of key findings from **SEH** and **SIEH** series

The designed molecules were synthesized, characterized by FTIR, ^{1}H, ^{13}C NMR, MS and HRMS analytical techniques and screened using *in vitro* enzyme inhibition assay. The results of *in vitro* assay indicate compound **SEH06** as most potent MAO-A inhibitor (IC_{50} = 0.053 ± 0.012 µM), compound **SIEH06** as most potent MAO-B inhibitor (IC_{50} = 0.024 ± 0.011 µM) while compound **SEH05** emerged as most potent AChE inhibitor (IC_{50} = 1.079 ± 0.104 µM). Compound **SIEH10** emerged as most selective MAO-B inhibitor and a well-balanced multifunctional molecule (MAO-A IC_{50} = 1.901 ± 0.102 µM, MAO-B IC_{50} = 0.034 ± 0.002 µM, AChE IC_{50} = 1.316 ± 0.013 µM and BChE IC_{50} = 9.827 ± 0.109 µM). BChE inhibitory activity of compound **SIEH10** was determined to evaluate the selectivity of the compound toward AChE. Enzyme kinetics and reversibility study shows the competitive irreversible nature of compound **SIEH10** towards MAO-B while mixed and

reversible inhibitor of AChE. Further, antioxidant and metal chelation studies of **SIEH10** indicate a high potential as an antioxidant and chelator of iron.

Additionally, the PAMPA-BBB assay of compound **SIEH10** indicates it as a CNS+ molecule while cell-based studies carried out against fibroblast (L929) and neuroblastoma (SH-SY5Y) cells to evaluate the toxicological profile of the *in vitro* lead compound **SIEH10** and were found to be non-toxic up to 10 μM concentration in fibroblast and toxic to neuroblastoma cells. Moreover, the *in vivo* results of the compound **SIEH10** against the scopolamine-induced amnesia model indicate that compound **SIEH10** is non-neuroprotective (**Figure 4.17**).